AWARD NUMBER: W81XWH-19-1-0126

TITLE: Reengineering of Antibiotics Informed by Antimicrobial Resistance Mechanisms

PRINCIPAL INVESTIGATOR: Dr. Matthew Belousoff

CONTRACTING ORGANIZATION: Monash University, Clayton, VIC, Australia

REPORT DATE: July 2021

TYPE OF REPORT: Final Report

PREPARED FOR: U.S. Army Medical Research and Development Command
Fort Detrick, Maryland 21702-5012

DISTRIBUTION STATEMENT: Approved for Public Release;
Distribution Unlimited

The views, opinions and/or findings contained in this report are those of the author(s) and should not be construed as an official Department of the Army position, policy or decision unless so designated by other documentation.

REPORT DOCUMENTATION PAGE

Form Approved
OMB No. 0704-0188

Public reporting burden for this collection of information is estimated to average 1 hour per response, including the time for reviewing instructions, searching existing data sources, gathering and maintaining the data needed, and completing and reviewing this collection of information. Send comments regarding this burden estimate or any other aspect of this collection of information, including suggestions for reducing this burden to Department of Defense, Washington Headquarters Services, Directorate for Information Operations and Reports (0704-0188), 1215 Jefferson Davis Highway, Suite 1204, Arlington, VA 22202-4302. Respondents should be aware that notwithstanding any other provision of law, no person shall be subject to any penalty for failing to comply with a collection of information if it does not display a currently valid OMB control number. **PLEASE DO NOT RETURN YOUR FORM TO THE ABOVE ADDRESS.**

1. REPORT DATE	2. REPORT TYPE	3. DATES COVERED
July 2021	Final Report	01Apr2019-31Mar2021

4. TITLE AND SUBTITLE
Reengineering of Antibiotics Informed by Antimicrobial

5a. CONTRACT NUMBER

5b. GRANT NUMBER
W81XWH-19-1-0126

5c. PROGRAM ELEMENT NUMBER

6. AUTHOR(S)

Matthew Belousoff

E-Mail: matthew.belousoff@monash.edu

5d. PROJECT NUMBER
PR180285

5e. TASK NUMBER

5f. WORK UNIT NUMBER

7. PERFORMING ORGANIZATION NAME(S) AND ADDRESS(ES)

Monash University, Wellington Rd, Clayton, VIC, 3800, Australia

8. PERFORMING ORGANIZATION REPORT NUMBER

9. SPONSORING / MONITORING AGENCY NAME(S) AND ADDRESS(ES)

U.S. Army Medical Research and Development Command
Fort Detrick, Maryland 21702-5012

10. SPONSOR/MONITOR'S ACRONYM(S)

11. SPONSOR/MONITOR'S REPORT NUMBER(S)

12. DISTRIBUTION / AVAILABILITY STATEMENT

Approved for Public Release; Distribution Unlimited

13. SUPPLEMENTARY NOTES

14. ABSTRACT

Report on progress of using cryo-electron microscopy as a tool to understand the key interactions that the oxazolidinone antibiotic family make with the bacterial ribosome as well as the means that the bacterial use to evolve resistance to this class of drugs.

15. SUBJECT TERMS
None listed.

16. SECURITY CLASSIFICATION OF:			17. LIMITATION OF ABSTRACT	18. NUMBER OF PAGES	19a. NAME OF RESPONSIBLE PERSON
a. REPORT	b. ABSTRACT	c. THIS PAGE			USAMRMC
Unclassified	Unclassified	Unclassified	Unclassified	36	19b. TELEPHONE NUMBER *(include area code)*

TABLE OF CONTENTS

1. Introduction

Wide-spread antibiotic use has driven the evolution of antimicrobial resistance (AMR), such that we are now in a critical period where available antibiotics are on the verge of obsolescence. Many have referred to this current lack of useable antibiotics as an 'Antibiotic Apocalypse', where deaths from previously treatable infections may soon exceed those of cancer and malaria. The pace at which new bacterial AMR strains emerge has created an urgent need for new strategies that can respond quickly to develop new disease management plans. We believe that we can re-engineer many current antibiotics that no longer work to make them effectively kill bacteria again. This greatly alleviates the time-consuming efforts and excessive costs of trying to discover "new" molecules or antibiotics. Our proposal is unique in that it combines a rational approach to antibiotic design with the relatively new technique of single particle cryogenic electron microscopy (Cryo-EM). Previously, these targets where too large for structural determination, hence the inability to determine the mode of resistance. Our program will revolutionize antibiotic discovery and production, as it uses specific information regarding how the bacteria have developed resistance to the original antibiotic, allowing immediate action to change the antibiotic to make it functional again.

2. Keywords

Antibiotics, linezolid, oxazolidinones, Anti-Microbial Resistance, Structure activity relationship, ribosome, drug design, cryo-electron microscopy

3. Accomplishments

a. What were the major goals of the project?

Aim 1. To determine the mutations that lead to linezolid-resistance in MRSA and VRE bacterial strains. Using clinical isolates we will determine their linezolid resistance mechanism by coupling whole genome sequencing, antibiotic susceptibility assays and cryoEM determination of their ribosomes.

Aim 2: To use ribosome structures to design and synthesize linezolid-related compounds for structure–activity relationship assessment

b. What was accomplished under these goals?

To answer this, I will address each aim separately:

Aim 1: To achieve a robust result in this we took a clinical isolate of MRSA which was susceptible to linezolid and ran a long term evolutionary selection experiment where we evolved the MRSA strain to become resistant to linezolid. Within three selection generations we were able to produce clonal isolates of MRSA which exhibited resistance to linezolid well beyond the clinical resistance break point (4 ug/mL). To analyse this data were utilized DNA deep sequencing to sequence all clonal isolates along the path to full linezolid resistance. This required sequencing 30 strains of MRSA of different clonal generations. This experiment has allowed us to gain a significant snapshot of the path that MRSA takes towards resistance to this clinically important antibiotic; linezolid.

Currently a manuscript is being prepared to report these results (see appendices). We found that the ribosomal mutations accumulated in a ribosomal protein called uL3 (which is adjacent to the antibiotic binding site). By studying the structure of one of the mutants using single particle cryoEM we were able to deduce the mechanism of resistance. Briefly the mutation rearranges the shape of this protein which has a coupling effect and propagates a structural change to the drug binding site, making the shape of the binding site no longer suitable for antibiotic binding. However, we also showed that this particular mutation has a drastic effect on the ability of the bacteria to thrive and demonstrated a growth defect in the resistant strain.

Major activities:

- Running long term evolutionary selection experiment

- Sequencing all relevant clonal isolates

- Bioinformatics to reconstruct genomes of all the clonal isolates and further analysis of evolutionary variation during course of experiment.

- Structural analysis of the linezolid resistant mutant by single particle cryo electron microscopy.

Aim 2: This aim has been largely achieved during the first year of this grant. Two separate publications have been published. The first describes the synthesis of different oxazolidinone (linezolid) derivates and their interaction with the bacterial ribosome. We were able to deduce the Structure activity relationship of the most potent derivatives which were synthesized. The second publication describes our efforts to synthesize 5 clinically relevant oxazolidinone derivatives and their subsequent analysis by cryoEM in complex with the ribosome from MRSA. In this this paper we clearly delineate the most important residues that these drugs make with the ribosome and show for the first time how a new drug which is in phase III clinical trials (contezolid) binds to the ribosome and what new contacts/interactions it makes.

Major activities:

- Organic synthesis of a variety of different oxazolidinone antibiotics

- MIC assays on new compounds with both MRSA and VRE

- Single particle cryoEM data collection on nearly 10 different antibiotic/ribosome complexes

- cryoEM data analysis and determination of structure activity relationships of all antibiotics in study

- preparation and publication of two manuscripts

c. **What opportunities for training and professional development has the project provided?**

Dr. Belousoff has been training a PhD student during the course of this grant, Alexander Wright. This student has been responsible for both the synthesis of new antibiotic compounds as well as the analysis of two cryoEM datasets. Alexander Wright is about to complete his PhD thesis and in the month of August 2021 gave his final PhD oration and is currently completing his PhD thesis.

Two masters rotation students have been trained in single particle cryoEM during this time and have been included as authors in the two publications.

d. **How were the results disseminated to communities of interest?**

Two publications that have been published during the first year of this project that speak directly to Aim 2:

Belousoff, Matthew J; Venugopal, Hari; Wright, Alexander; Seoner, Samuel; Stuart, Isabella; Stubenrauch, Chris; Bamert, Rebecca S; Lupton, David W; Lithgow, Trevor; *cryoEM-Guided Development of Antibiotics for Drug-Resistant Bacteria*, **ChemMedChem**, 14 (5) , 527-531, 2019

Wright, Alexander; Deane-Alder, Kieran; Marschall, Edward; Bamert, Rebecca; Venugopal, Hari; Lithgow, Trevor; Lupton, David W; Belousoff, Matthew; *Characterization of the core ribosomal binding region for the oxazolidone family of antibiotics using Cryo-EM*, **ACS Pharmacology & Translational Science,** 2020

Laura Perlaza, Kher-shing Tan, Sarah Piper, Rachel Johnson, Rebecca Bamert, Alexander Wright, David Lupton, Trevor Lithgow, Matthew J. Belousoff *A structurally characterized Staphylococcus aureus evolutionary escape route from treatment with the antibiotic linezolid.* **Manuscript in Preparation**

The work was also presented as a poster at the Lorne Proteins 2020 conference.

e. **What do you plan to do during the next reporting period to accomplish the goals?**

Not applicable

4. Impact

a. **What was the impact on the development of the principal discipline(s) of the project?**

The main impact of the successful outcomes of Aim 1 were the following:

- We were able to show that early evolution of antibiotic resistance in *Staph. aureus* appears to begin with ribosomal mutations to allow immediate antibiotic escape. This comes at a significant fitness cost, so perhaps acquiring resistance genes is a longer term strategy that allows bacteria to retain fitness as well as antibiotic resistance

- We were able to demonstrate the mechanism by which a particular mutation/s abolish binding by the antibiotic linezolid by solving the structure of the antibiotic resistant ribosome isolated. We showed that a distant mutation in a ribosomal protein is sufficient to rearrange the drug binding site enough to lower the affinity of the drug to its binding site.

The main impact of the successful outcomes of Aim 2 were the following:

- We were able to conclusively determine the key residues in the drug binding site of the oxazolidinone antibiotic family within the ribosome from methicillin resistant *Staph. aureus* (**ACS Pharmacology and Translational Science**, 2020). This achievement is a significant step towards successful reengineering of this class of antibiotics as we have shown the key binding residues to focus efforts on.

- Moreover in we have shown that it is possible to make minor modifications to linezolid to both improve its binding properties to the ribosome and increase its ability to inhibit bacterial replication (**ChemMedChem**, 2019).

b. **What was the impact on other disciplines?**

To date there have been few examples of using cryoEM as a drug development tool. In our two publications we clearly show the utility of this new technique to understand drug/target interactions at the molecular level.

c. **What was the impact on technology transfer?**

Nothing to report.

d. **What was the impact on society beyond science and technology?**

Nothing to report.

5. Changes/Problems

Due to the constant COVID-19 lockdowns in Melbourne, Australia (~250 days) during the course of the grant period, our initial plans to study a series of linezolid resistant strains from local hospitals was not able to be performed. This was due to a large shift in focus of the microbiology departments at these hospitals during this time as well as the lack of ability to be in the laboratory and the need to power down our electron microscopes. However, to compensate for this we did perform the antibiotic evolutionary study in order to try and address Aim 1.

6. Products

The major products so far from this research projects are two peer reviewed journal articles:

Belousoff, Matthew J; Venugopal, Hari; Wright, Alexander; Seoner, Samuel; Stuart, Isabella; Stubenrauch, Chris; Bamert, Rebecca S; Lupton, David W; Lithgow, Trevor; *cryoEM-Guided Development of Antibiotics for Drug-Resistant Bacteria*, **ChemMedChem**, 14 (5) , 527-531, 2019

Wright, Alexander; Deane-Alder, Kieran; Marschall, Edward; Bamert, Rebecca; Venugopal, Hari; Lithgow, Trevor; Lupton, David W; Belousoff, Matthew; *Characterization of the core ribosomal binding region for the oxazolidone family of antibiotics using Cryo-EM*, **ACS Pharmacology & Translational Science,** 2020

7. Participants & Other Collaborating Organizations

Name:	*Alexander Wright*
Project Role:	*Graduate Student*
Researcher Identifier (e.g. ORCID ID):	
Nearest person month worked:	12
Contribution to Project:	*Mr. Wright performed all the organic chemistry synthesis for Aim 2 and has also analysed two cryoEM datasets.*
Funding Support:	*Mr. Wright is supported by the School of Chemistry, Monash University for his PhD stipend*

Name:	*Rebecca Bamert*
Project Role:	Staff scientist
Researcher Identifier (e.g. ORCID ID):	
Nearest person month worked:	12 (4 days a week)
Contribution to Project:	*Ms. Bamert performed the evolutionary selection experiments, prepared clonal isolates for sequencing. She also helped analyse the cryoEM data and prepare samples.*
Funding Support:	*Ms. Bamert was supported by this research grant.*

8. Special Reporting Requirements

Not applicable

9. Appendices

PDF copy of both published manuscripts and the manuscript draft are attached.

ACS Pharmacology & Translational Science

pubs.acs.org/ptsci

Letter

Characterization of the Core Ribosomal Binding Region for the Oxazolidone Family of Antibiotics Using Cryo-EM

Alexander Wright, Kieran Deane-Alder, Edward Marschall, Rebecca Bamert, Hari Venugopal, Trevor Lithgow,* David W. Lupton,* and Matthew J. Belousoff*

Cite This: *ACS Pharmacol. Transl. Sci.* 2020, 3, 425−432

Read Online

ACCESS | Metrics & More | Article Recommendations | Supporting Information

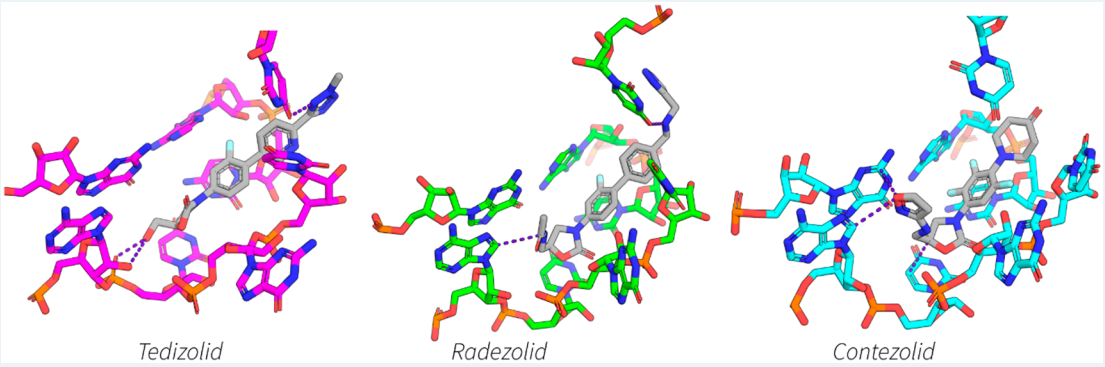

ABSTRACT: Linezolid and tedizolid are oxazolidinones with established clinical utility for the treatment of Gram-positive pathogens. Over time it has become apparent that even modest structural changes to the core phenyl oxazolidinone leads to drastic changes in biological activity. Consequently, the structure−activity relationship around the core oxazolidinone is constantly evolving, often reflected with new structural motifs present in nascent oxazolidinones. Herein we describe the use of cryo-electron microscopy to examine the differences in binding of several functionally different oxazolidinones in the hopes of enhanced understanding of their SAR. Tedizolid, radezolid, T145, and contezolid have been examined within the peptidyl transferase center (PTC) of the 50S ribosomal subunit from methicillin resistant *Staphylococcus aureus*. The ribosome−antibiotic complexes were resolved to a resolution of around 3 Å enabling unambiguous assignment of how each antibiotic interacts with the PTC.

KEYWORDS: *antibiotics, linezolid, contezolid, oxazolidinones, cryo-EM, ribosome*

Downloaded via MONASH UNIV on August 17, 2021 at 04:20:01 (UTC).
See https://pubs.acs.org/sharingguidelines for options on how to legitimately share published articles.

Linezolid (**1**) was the first oxazolidinone antimicrobial agent developed, and is the first purely synthetic antibiotic known.[1−3] Its potency against all major Gram-positive pathogens, including newer multidrug resistant strains such as methicillin resistant *Staphylococcus aureus* (MRSA) and vancomycin-resistant enterococci (VRE), have ensured it has gained a significant place as a last line antibiotic.[4] Oxazolidinones act as protein synthesis inhibitors, binding in the 23S rRNA region adjacent to the PTC within the 50S subunit.[5] They bind directly in the A-site position of where the 5′ amino acylated tRNA docks, thereby sterically hindering any incoming tRNA substrates into the enzymatic core of the ribosome.[6] This novel mode of action results in a remarkable absence of cross-resistance between linezolid (**1**) and other antimicrobials.[7] This lack of cross-resistance is paramount to the success of linezolid (**1**) given the emergence of multidrug resistant pathogens. Despite such promising features, safety limitations surrounding linezolid (**1**) have limited the expansion of the oxazolidinone family of antimicrobials.[7−9] The reasoning behind this is attributed to the homology between the 23S ribosomal target and the closely related mitochondrial protein synthesis processes in mammals,[5,7,10,11] thereby resulting in adverse effects such as myelosuppression and monoamine oxidase (MAO) inhibition.[7,10,12] Despite these limitations over the last decades a number of oxazolidinone antimicrobials have been developed based on linezolid (**1**) with modifications in the C5-domain, B-ring, C-ring, and addition of a D-ring (Figure 1a).

Since the discovery of linezolid (**1**) over two decades ago, the only other oxazolidinone to be clinically approved is tedizolid (**2**).[13] Considering the manifold efforts into the discovery of oxazolidinone antimicrobials it is somewhat surprising that only two successful analogues have been uncovered. Of the thousands of oxazolidinones synthesized many boast greater

Special Issue: Antibiotics

Received: April 30, 2020
Published: May 13, 2020

ACS Publications

© 2020 American Chemical Society

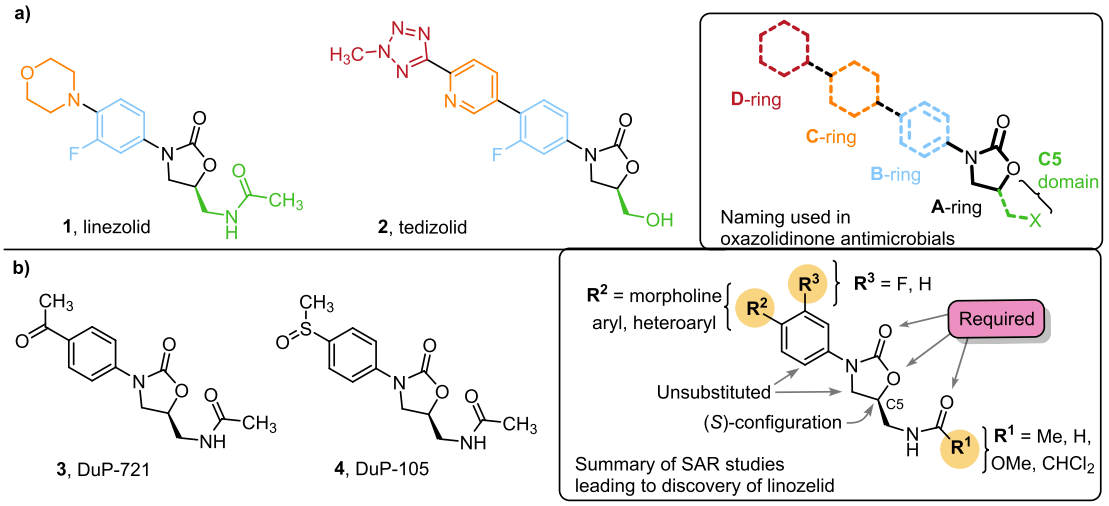

Figure 1. (a) Structure of the two clinically approved oxazolidinone antibiotics, linezolid (**1**) and tedizolid (**2**). On the right is the naming convention of the oxazolidinone chemical extensions. (b) The two precursor DuPont compounds DuP-721 (**3**) and DuP-105 (**4**), on the right is the general SAR approach for the first generation of oxazolidinone antibiotics.

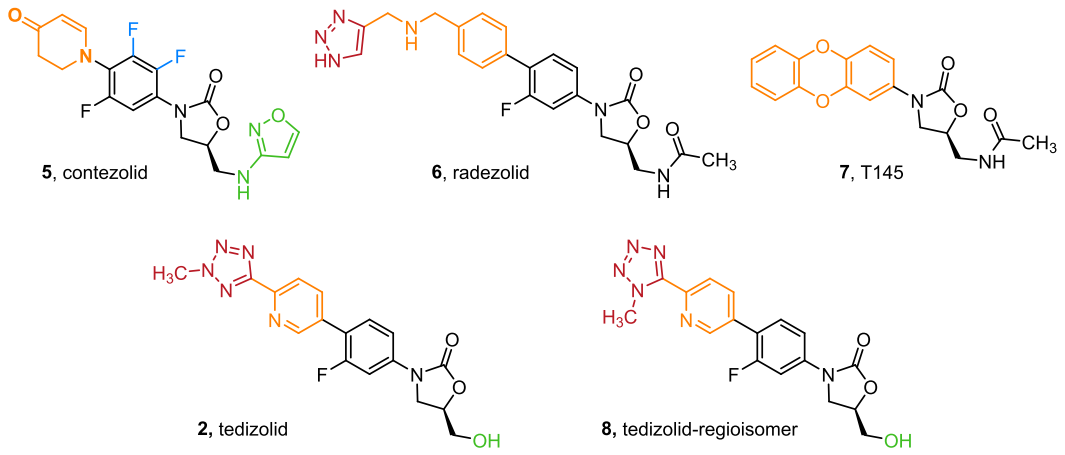

Figure 2. Oxazolidinone compounds synthesized and used in the cryo-EM study.

antibacterial properties than linezolid (**1**) and even tedizolid (**2**).[14] However, increased toxicity due to mitochondrial binding is often associated with greater antimicrobial potency, and is rarely addressed. In more recent times the focus around the synthesis of oxazolidinones has shifted from potency, prioritizing an improved safety profile.[15]

Structure−activity relationships (SAR) are an essential tool in the discovery of new antimicrobials. Over the extended period in which oxazolidinone antimicrobials have been developed the SAR has evolved, presenting new opportunities for the introduction of functional motifs with, increasingly, a focus on reducing toxicity. Long before linezolid (**1**) was received clinically, the SAR of oxazolidinone based antimicrobials had been explored by DuPont.[16,17] The pioneering work culminated with the first clinical candidate oxazolidinones DuP-721 (**3**) and DuP-105 (**4**).[16,17] However, DuPont discontinued research into these progenitor oxazolidinones due to concerns with animal toxicity. Scientists at Upjohn Co. later continued the investigation culminating in the initial discovery of linezolid (**1**) which received regulatory approval in the early 2000s (Figure 1b).[13]

DuPont's extensive SAR research, allowed the eventual identification of linezolid (**1**) as a therapeutic agent. The SAR gave a generalized guide for the synthesis for novel oxazolidinones that remains important to this day. Specifically, it was demonstrated that the A-ring oxazolidinone core should have (*S*) chirality, while acetamide or substituted acetamide (R^1) were the optimal substituents for the C5-domain with larger structures reducing biological activity.[17,18] The B-ring system often retains substituents *meta* and *para* to the amine, while a C-ring (R^2) can be tolerated.

Some 14 years after the discovery of linezolid (**1**) the next successful clinical candidate, tedizolid, was developed. First synthesized in 2011, tedizolid (**2**) is a second generation oxazolidinone and one of a few pyridyl phenyl derivatives found to have improved biologically activity.[19] However, these analogues often suffer from low bioavailability and insolubility requiring alteration of the C5-domain to incorporate a phosphate prodrug approach.[20] The pyridyl phenyl motifs extended typical C-ring modification by the addition of a D-ring. Yoon et al. demonstrated that these D-ring systems impacted the C5-domain thereby allowing functionality other than the archetypal acetamide reported by DuPont to be introduced (see Figure 1).[20]

Before the discovery of tedizolid (**2**) problems with toxicity had become apparent with oxazolidinone antimicrobials. In

https://dx.doi.org/10.1021/acsptsci.0c00041
ACS Pharmacol. Transl. Sci. 2020, 3, 425−432

Scheme 1. Synthesis of Oxazolidinone 13 by a Procedure Modified from Yoon et al.[a]

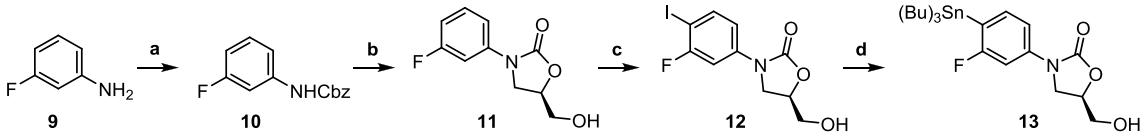

[a]Reagents and conditions: (a) K_2CO_3, Cbz-Cl, THF/H_2O, 0 °C to rt; (b) n-BuLi, (*R*)-glycidyl butyrate, THF, −78 °C to rt; (c) NIS, TFA, rt; (d) $(Bu)_3Sn-Sn(Bu)_3$, $Pd(PPh_3)_2Cl_2$, dioxane, 100 °C.[20]

Scheme 2. Synthesis of Tetrazoles 16 and 17 by a Procedure Modified from Yoon et al.[a]

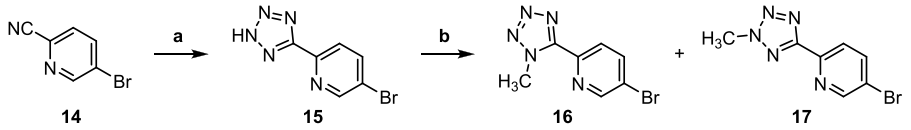

[a]Reagents and conditions: (a) NaN_3, $ZnCl_2$, pyridine, reflux; (b) CH_3I, NaOH, DMF, 0−40 °C.[20]

Scheme 3. Synthesis of Tedizolid (2) and Regiosimer 8 by a Procedure Modified from Yoon et al.[a]

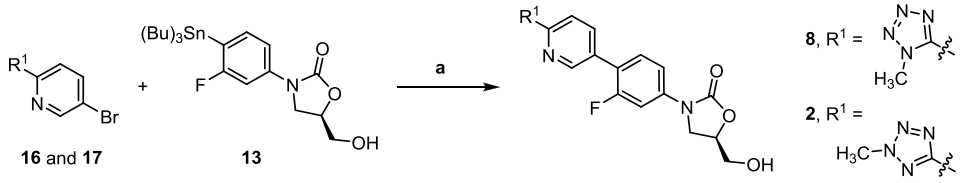

[a]Reagents and conditions: (a) $Pd(PPh_3)_2Cl_2$, LiCl, NMP, 120 °C.[20]

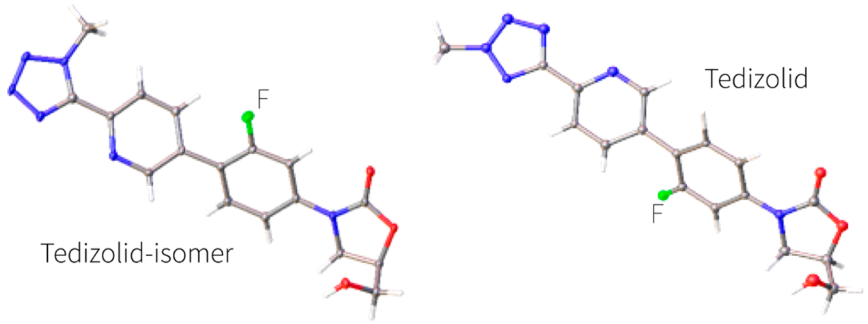

Figure 3. X-ray crystal structures from this study of tedizolid (**2**) (right) and its regioisomer **8** (left), both compounds are very close in structure except for the relative position of the fluorinated benzene in the B-ring which is rotated 180° between each structure.

2005 Barbachyn reported the first example of B-ring modifications leading to an improved safety profile.[1,7] However, altered B-ring oxazolidinones had previously made little progress as potential therapeutics. It wasn't until 2014 when Gordeev et al. demonstrated the potential of fluorinated B-ring systems which lead to the discovery of contezolid.[7] This novel oxazolidinone maintained anti MRSA potency while having an improved safety profile, halving myelosuppression and reducing MAO inhibition by a third.[1,7] Accelerated development of contezolid allowed entry to phase III trials in late 2019 with promising results and the potential to replace linezolid (**1**). Studies by Gordeev et al. showed that trisubstituted B-ring systems often suffer from a reduction in antimicrobial activity.[7] However, by simultaneously modifying the C-ring and C-5 domain, improved minimum inhibitory concentration (MIC) values could be retained along with the desired safety profile.

The development of oxazolidinones antimicrobials presents a challenge with a delicate balance between antimicrobial activity and toxicity required. The addition of a D-ring enables changes to the C-5 domain invoking a different mode of binding within the ribosomal subunit. This is also apparent for trisubstituted B-ring systems such as contezolid (**5**), where the C5-domain acetamide was changed to an isoxazaole to retain its MIC. Furthermore, D-ring systems or indeed extended C-ring systems such as those in tedizolid (**2**) and radezolid (**6**) exhibit binding to the periphery of the PTC previously unseen. Thus, while the oxazolidinone antimicrobials retain a common mode of action their interactions with the PTC appear to be suitably perturbed by various structural changes. To gain both a better understanding of how oxazolidinone structure impacts PTC binding, and to further develop the use of cryo-EM as a tool in structure-based drug design, we have examined the oxazolidinones, contezolid (**5**), radezolid (**6**), T145 (**7**), tedizolid (**2**), and a regioisomer of tedizolid (**8**), using cryo-EM (Figure 2). From this study it has been possible to clearly map the main sites of interaction, and highlight chemical differences in these drugs and how they lead to different interactions in the binding site. Moreover, our results show that by comparing the binding mode of four different oxazolidinones we can more accurately

https://dx.doi.org/10.1021/acsptsci.0c00041
ACS Pharmacol. Transl. Sci. 2020, 3, 425−432

Scheme 4. Proposed Synthesis of T145 (7) by Ippoliti et al. Showing Modifications in the Sequence[a]

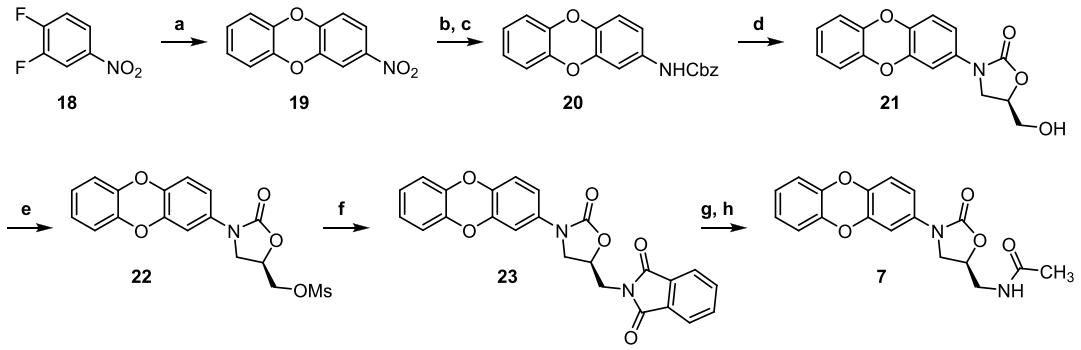

[a]Reagents, and conditions: (a) Catechol, K_2CO_3, DMF, 100 °C; (b) Pd/C, H_2, THF, rt; (c) Cbz-Cl, $NaHCO_3$, THF/H_2O, rt; (d) LiHMDS, (R)-glycidyl butyrate, THF, −78 °C to rt; (e) MsCl, Et_3N, CH_2Cl_2, 0 °C to rt; (f) K-Phth, DMF, 90 °C; (g) $N_2H_4{\cdot}H_2O$, EtOH, reflux; (h) AcO_2, Et_3N, CH_2Cl_2, 0 °C to rt.[22]

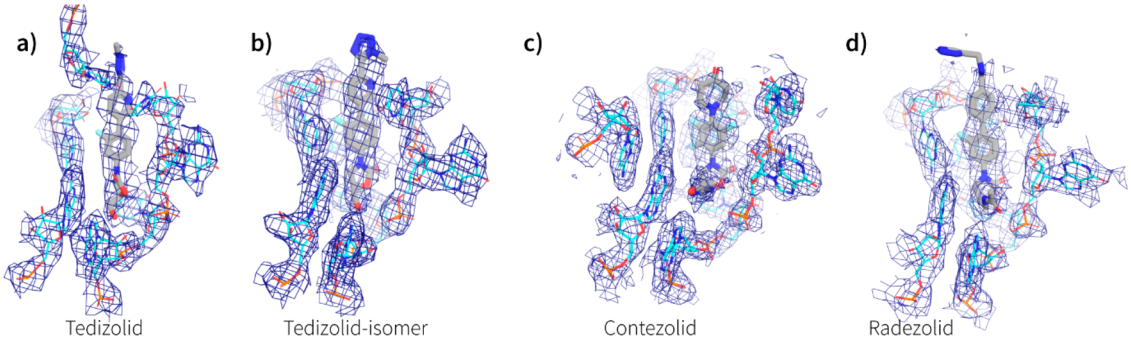

Figure 4. Calculated densities around the antibiotic binding site: (a) tedizolid; (b) tedizolid-regioisomer; (c) contezolid; and (d) radezolid. All density is drawn at 4 σ and the binding site is drawn from the same relative ribosome orientation.

determined the "core" residues that compose the binding pocket for this important class of drugs.

RESULTS AND DISCUSSION

Synthesis of Oxazolidione Compounds. To allow a comprehensive cryo-EM study into oxazolidinone antimicrobials most of these needed to be synthesized. Tedizolid (**2**) was prepared following a synthetic procedure described by Yoon et al.[20] with minor modifications. Specifically, coupling of stannane **13** (Scheme 1) with a mixture of tetrazoles **16** and **17**, themselves prepared in two steps from pyridine **14** (Schemes 2 and 3), gave tedizolid (**2**) and the regioisomeric compound **8**. While originally intended to deliver tedizolid alone, formation of **8** was considered fortuitous as it would allow the impact the site of methylation has on ribosome binding to be examined. To unambiguously determine the structures of tedizolid (**2**) and its isomer **8**, two X-ray crystal structures were determined to ensure the integrity of the final compounds used for the cryoEM studies (Figure 3).

Radezolid (**6**) was synthesized following procedures defined by Shili et al.[21] albeit with the key Suzuki coupling requiring an increased catalyst loading. While the synthesis of contezolid (**4**) was achieved following a sequence described by Gordeev et al.,[7] oxazolidinone formation was achieved using LiHMDS instead of LiO^tBu. Finally, oxazolidinone T145 (**7**) was prepared using the procedure proposed by Ippoliti et al.;[22] however, amide formation exploited a Gabriel synthesis rather than working from an azide (Scheme 4).

Cryo-EM Determination of Ribosome/Antibiotic Complexes. To better understand the precise binding mode of these members of the oxazolidinone family of antibiotics with their cognate target, the bacterial ribosome, we employed single particle cryo-EM. The structures were achieved by combining dimethyl sulfoxide (DMSO) solubilized antibiotic (final concentration ∼10 μM) to freshly thawed 70S ribosomes isolated from MRSA. This solution was allowed to incubate at 37 °C for 15 min, on ice for 1 h, then immediately applied to glow discharged TEM grids and plunge frozen with liquid ethane. All specimens were imaged at an acceleration voltage of 200 kV. While specimens contained the 70S ribosomes, only the 50S ribosomal subunit was subjected to final refinement in RELION or cryoSPARC (see methods section), in order to achieve the highest possible resolution.

The density observed around the oxazolidinone binding site allowed for unambiguous placement of every antibiotic (see Figure 4) except for T145, which only showed density for the lower part of the B-ring and C5-domain (see Supporting Information, Figure S2). For this reason, T145 will be left out of further discussions. The binding site of the oxazolidinones is remarkably similar to that previously described[4,6,23] and is at the A-site of the PTC, completely encapsulated by rRNA (see Figures 4 and 5).

Tedizolid (**2**) with the extended C-ring consisting of a pyridine and methylated tetrazole still retains a classical oxazolidinone binding pose, but with subtle differences. The tetrazole enables a close lone-pair interaction (3 Å away) between the tetrazole and U2584 (*E. coli* rRNA numbering used throughout) (see Figure 5a), and as the C5-domain substituent is only a hydroxyl group it forms two possible hydrogen-bond contacts with the phosphate oxygen and the ribose 2′-OH of

https://dx.doi.org/10.1021/acsptsci.0c00041
ACS Pharmacol. Transl. Sci. 2020, 3, 425−432

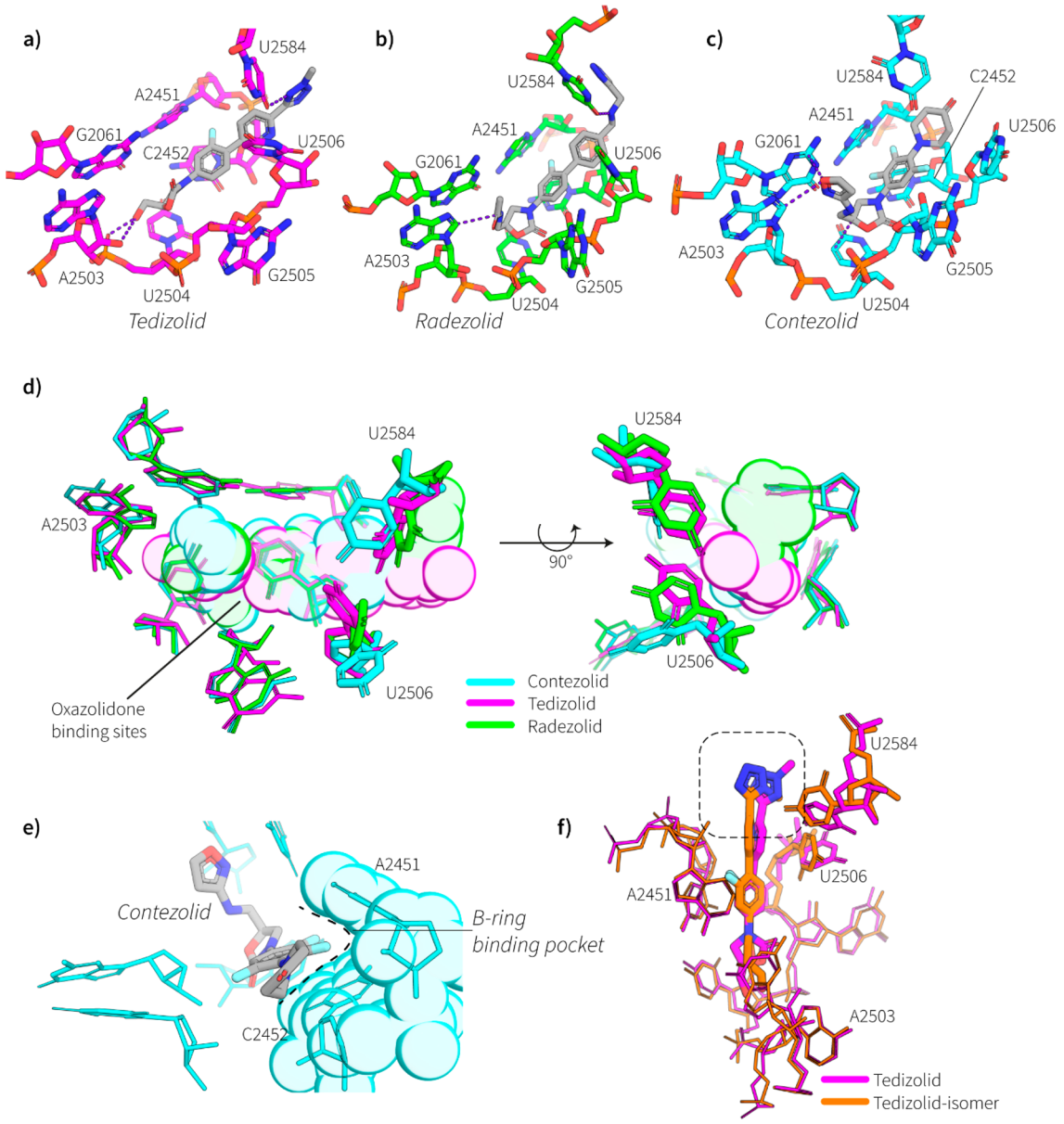

Figure 5. Cartoon representation of the binding site of the different oxazolidinone derivatives in the PTC of the 50S subunit of the MRSA ribosome. (a) Binding site of tedizolid (**2**), showing hydrogen bonds as dashed blue lines between the tedizolid hydroxyl and the backbone of A2503 and an interaction between the tedizolid tetrazole and U2584. (b) Binding site of radezolid (**6**) showing a van-der Waals interaction between the radezolid acetyl group and the purine nucleobase A2503, and a hydrogen bond with the secondary amine and U2584, shown as dashed blue lines. (c) Binding site of contezolid (**5**) highlighting $\pi-\pi$ interactions between the isoxazole in the C5-domain of contezolid with G2061 and a van der Waals interaction with A2503, shown as a dashed blue line is also a tighter interaction of the oxazolidinone with the nucleobase of U2504. (d) Overlay of binding site and relative orientations of the rRNA nucleotides of contezolid (cyan), radezolid (green), and tedizolid (magenta), the oxazolidinones are shown as a translucent cloud. Highlighted in bolder sticks are the nucleotides that exhibit the greatest conformational change depending on the oxazolidinone bound. (e) View of the B-ring binding pocket defined by A2451 and C2452 which nestles the fluorinated benzene of contezolid (**5**). (f) Overlay of both the tedizolid (**2**) (magenta) and tedizolid-regioisomer **8** (orange) ribosome binding site. Highlighted in bolder sticks is the two nucleobases that change the most in conformation between the two structures (U2584 and U2506), which are presumably disturbed by the position of the methyl group (highlighted in dashed box) which slightly offsets the binding position of the isomer relative to clinically used, tedizolid (**2**).

A2503. The comparison of tedizolid (**2**) with the methyl tetrazole regioisomer **8** is also of interest. The regioisomer of tedizolid places the methyl group in an unfavorable position which abolishes the lone-pair interaction with U2584, causing rearrangement of both U2584 and U2506, which moves in closer to the binding site of the tedizolid-regioisomer **8** (see Figure 5f).

Radezolid (**6**) also has a C-ring extension and binds in a very similar pose to tedizolid (**2**), and utilizes the secondary amine in the C-ring to form a hydrogen bond with the uracil nucleobase U2584, which in turn brings the nucleotide closer to the aromatic triazole moiety opening up the potential for $\pi-\pi$ interactions between U2584 and the triazole (see Figure 5b,d). The acetyl substituent in the C5-domain adopts a similar pose as compounds previously studied in our group,[4] which directs toward A2503 for a van-der Waals interaction with the adenosine nucleobase.

https://dx.doi.org/10.1021/acsptsci.0c00041
ACS Pharmacol. Transl. Sci. 2020, 3, 425−432

Contezolid (**5**), while not having such a long C-ring modification, replaces the morpholine (as found in linezolid (**1**)) with a piperidinone which does not appear to make any extra contacts with either U2584 or U2506, both of which seem to change conformations significantly when contezolid (**5**) is bound (see Figure 5c,d), both nucleotides orientating further from the oxazolidinone binding pocket. However, the C-ring also has a trifluorinated benzyl group which nestles in further to the hydrophobic pocket defined by the nucleotides A2451 and C2452 (see Figure 5e), also the isoxazole in the C5-domain makes new contacts with both G2061 (a $\pi-\pi$ interaction) and A2503 (a van der Waals interaction).

Oxazolinones represent a crucial chemical functionality in the development of new antimicrobial agents. Their use however has been marred by toxicity and relatively high minimatory inhibition concentrations (MIC). Efforts to improve on linezolid (**1**) have led to compounds like tedizolid (**2**) and radezolid (**6**) which sought to improve efficacy by expanding the C-ring portion of the chemical in an effort to maximize contacts within the ribosomal binding pocket. This study shows that these efforts have yielded results with tedizolid having over a 10 time better MIC than linezolid (**1**)[24] which is most likely due to the increased contacts that the C-ring has with both U2506 and U2584 as well as the extra hydrogen bonds between the 5′-OH and A2503. The enhanced efficacy of radezolid (**6**)[25] compared to linezolid (**1**) is also most likely due to the extra contacts the C-ring triazole extension makes with U2584 as well as the secondary amine.

It seems that the regioisomer of tedizolid while binding a very similar pocket to its clinical counterpart, perhaps makes some deleterious interactions due to the positioning of the methyl group on the tetrazole, most likely the reason why this compound was abandoned. Tedizolid (**2**) also shows that extensions in the C5-domain may be unnecessary for efficacy, but when compared to contezolid (**5**), perhaps plays a part in toxicity and selective binding to bacterial vs mitochondrial ribosomes.

Design choices during the development of contezolid (**5**), one of the newest members of the oxazolidione family, seem to have avoided inclusion of C-ring expansions. This is most likely due to the poor solubility associated with greater aromatic functionality which seems critical to binding, and adjustments have been made to the B-ring, by adding extra fluorines to the core benzyl group. Our cryo-EM results suggest that this allows this portion of the drug to nestle in a hydrophobic pocket defined by A2451 and C2452. While this interaction is not novel compared to other members of the family, combination with the isoxazole in the C5-domains clearly allows this compound to bind effectively (4 fold enhanced MIC than linezolid (**1**)) and endows the drug with a higher efficacy compared to linezolid (**1**) with seemingly less associated toxicity. When contezolid (**5**) binds to the ribosome it seems to reflect that making interactions with U2584 and U2506 is not crucial for oxazolidinone function and that the core binding site consists of the residues G2061, A2503, U2504, G2505, A2451, and C2452. Any new oxazolidinone drugs should potentially focus efforts in improving interactions with these core residues.

MATERIALS AND METHODS

Purification of Ribosomes from MRSA. Ribosomes were isolated as previously described.[4]

X-ray Crystallography. Single crystals of tedizolid and tedizolid-regioisomer were grown by the vapor diffusion method, diffusing *n*-pentane into a dichloromethane/methanol (1:1) solution of the antibiotic. A suitable crystal was selected and collected on a XtaLAB Synergy, Dualflex, HyPix diffractometer. The crystal was kept at 123.00(10) K during data collection. Using Olex2,[26] the structure was solved with the ShelXT structure solution program using Intrinsic Phasing and refined with the ShelXL[27,28] refinement package using Least Squares minimization. See Table S2 for crystallographic parameters.

Electron Microscopy. Cryo-EM samples were prepared by plunge vitrification in liquid ethane on a Vitrobot Mark IV (Thermo Fisher Scientific) with a blotting chamber set to 4 °C and 100% humidity. A 3 μL aliquot of the sample solution was applied on Quantifoil R1.2/1.3 Cu 200 mesh (Quantifoil) glow-discharged grids and blotted for 1.5 s before the grid was plunged. Data were collected on a Glacios or Artica (see Supporting Information, Table S1) (Thermo Fisher Scientific) 200 kV electron microscope equipped with a Falcon 3 direct electron detector. The microscope was set with a 50 μm condenser aperture, no objective aperture, spot at 6, and beam diameter of 2.4 μm. The equivalent pixel size on the detector was either in the range between 0.874−1.14 Å/pixel depending on the specimen (see Supplemental Table S1). The total electron dose was either 47 or 50 e.Å^{-2} with an expose time of either 47 or 50 s. Multiframe movies were automatically acquired with the EPU software package (Thermo Fisher Scientific) in gain-normalized uncompressed MRC format with a 9-position beam-image shift data acquisition scheme and target defocus range of 0.4 to 1.6 μm.

Data Processing. Movies were motion-corrected, dose-weighted, and integrated using UCSF MotionCor2.[29,30] This was followed by CTF estimation using the GCTF[31] software package. Particles were picked from the micrographs using the automated procedure in the crYOLO software package.[32,33] Particle extraction and reference-free 2D classification was carried out in RELION (version 3.0.7).[34] Initial 3D references were used from a previous study[4] and used for 3D classification in RELION. A homogeneous subset of particles was then subjected to cycles of Bayesian particle polishing and CTF refinement as implemented in RELION. This homogeneous subset of polished particles was used for a 3D refinement in RELION and was further classified into 3D classes with a fine grain angular sampling only allowing for local Euler angle searches. Particles belonging to the 3D class were further refined in RELION (version 3.1) where their higher order CTF parameters were rerefined taking into account particles belonging to each image shift group. Further 3D refinements where the 30S subunit was masked and a final 3D refinement was carried out in RELION (version 3.1), yielding consensus maps of the complex at a global resolution (FSC = 0.143) of between 2.9 and 3.2 Å (see Table S1). For the tedizolid regioisomer **8**, the final refinement was carried out in cryoSPARC[35] using their nonuniform refinement strategy, with a mask that covered the 50S subunit.

Atomic Model Refinement. The 50S models were all based on PDB: 6DDD[4] which was used as the initial PDB template. All models were flexibly fitted into the EM density maps using the molecular dynamics flexible fitting (MDFF) simulation with nanoscale molecular dynamics (NAMD).[36] These models were then subjected to real-space refinement, as implemented in the PHENIX software package.[37] Refinement restraints for each antibiotic were generated in eLBOW routine in PHENIX and placed and manually refined in coot.[38] After iterative refinement

https://dx.doi.org/10.1021/acsptsci.0c00041
ACS Pharmacol. Transl. Sci. 2020, 3, 425−432

and manual adjustments, comprehensive validation implemented in PHENIX was performed to assess the model quality as presented in Table S1.

Structure statistics are detailed in Table S1.

Figures. All figures were generated in PyMOL.[39]

Data Availability. The cryo-EM density maps were deposited in the Electron Microscopy Data Bank under accession codes EMD-21872, EMD-21873, EMD-21887, and EMD-21888 for contezolid-50S, radezolid-50S, tedizolid-50S, and tedizolid-regioisomer-50S, respectively. The PDB coordinates were deposited in the PDB database under the accession codes 6WQN, 6WQQ, 6WRS, and 6WRU for contezolid-50S, radezolid-50S, tedizolid-50S, and tedizolid-regioisomer-50S, respectively.

■ ASSOCIATED CONTENT

Supporting Information

The Supporting Information is available free of charge at https://pubs.acs.org/doi/10.1021/acsptsci.0c00041.

Full synthetic methods for the antibiotic synthesis, tables containing the cryo-EM and X-ray structure statistics, and figures for the Fourier shell correlation (FSC) curves of each structure (PDF)

■ AUTHOR INFORMATION

Corresponding Authors

Trevor Lithgow − *Infection & Immunity Program, Monash Biomedicine Discovery Institute and Department of Microbiology, Monash University, Clayton 3800, Victoria, Australia*; Email: trevor.lithgow@monash.edu

David W. Lupton − *School of Chemistry, Monash University, Clayton 3800, Victoria, Australia*; orcid.org/0000-0002-0958-4298; Email: david.lupton@monash.edu

Matthew J. Belousoff − *Drug and Development Biology, Monash Institute of Pharmaceutical Sciences, Monash University, Parkville 3052, Victoria, Australia*; orcid.org/0000-0002-3229-474X; Email: matthew.belousoff@monash.edu

Authors

Alexander Wright − *School of Chemistry, Monash University, Clayton 3800, Victoria, Australia*

Kieran Deane-Alder − *Drug and Development Biology, Monash Institute of Pharmaceutical Sciences, Monash University, Parkville 3052, Victoria, Australia*

Edward Marschall − *Department of Biochemistry and Molecular Biology, Monash University, Clayton 3800, Victoria, Australia*

Rebecca Bamert − *Infection & Immunity Program, Monash Biomedicine Discovery Institute and Department of Microbiology, Monash University, Clayton 3800, Victoria, Australia*

Hari Venugopal − *Ramaciotti Center for Cryo-Electron Microscopy, Monash University, Clayton 3800, Victoria, Australia*

Complete contact information is available at: https://pubs.acs.org/10.1021/acsptsci.0c00041

Funding

This work was supported by a grants from US-DOD (PRMRP: W81XWH1910126) for M.J.B. and by the National Health & Medical Research Council of Australia (Program Grant 1092262 to T.L.) and the Australia Research Council (DP 170103567 to D.W.L.). The funders had no role in study design, data collection, and interpretation, or the decision to submit the work for publication. We acknowledge the support of the Ramaciotti Center for Electron Microscopy for the data collection on the Artica and for Thermo Scientific for the Glacios housed in Prof. Patrick Sexton's laboratory. This work was supported by the MASSIVE HPC facility (www.massive.org.au).

Notes

The authors declare no competing financial interest.

■ REFERENCES

(1) Fisher, J. F., Mobashery, S., and Miller, M. J (2018) *Antibacterials*, Vol. II, Topics in Medicinal Chemistry , 26, Springer.

(2) Brickner, S. J., Barbachyn, M. R., Hutchinson, D. K., and Manninen, P. R. (2008) Linezolid (ZYVOX), the first member of a completely new class of antibacterial agents for treatment of serious gram-positive infections. *J. Med. Chem. 51* (7), 1981−90.

(3) Ford, C. W., Zurenko, G. E., and Barbachyn, M. R. (2001) The discovery of linezolid, the first oxazolidinone antibacterial agent. *Curr. Drug Targets: Infect. Disord. 1* (2), 181−99.

(4) Belousoff, M. J., Venugopal, H., Wright, A., Seoner, S., Stuart, I., Stubenrauch, C., Bamert, R. S., Lupton, D. W., and Lithgow, T. (2019) cryoEM-Guided Development of Antibiotics for Drug-Resistant Bacteria. *ChemMedChem 14*, 527.

(5) Belousoff, M. J., Eyal, Z., Radjainia, M., Ahmed, T., Bamert, R. S., Matzov, D., Bashan, A., Zimmerman, E., Mishra, S., Cameron, D., Elmlund, H., Peleg, A. Y., Bhushan, S., Lithgow, T., and Yonath, A. (2017) Structural Basis for Linezolid Binding Site Rearrangement in the Staphylococcus aureus Ribosome. *mBio 8* (3), 821−32.

(6) Eyal, Z., Matzov, D., Krupkin, M., Wekselman, I., Paukner, S., Zimmerman, E., Rozenberg, H., Bashan, A., and Yonath, A. (2015) Structural insights into species-specific features of the ribosome from the pathogen Staphylococcus aureus. *Proc. Natl. Acad. Sci. U. S. A. 112* (43), E5805−14.

(7) Gordeev, M. F., and Yuan, Z. Y. (2014) New potent antibacterial oxazolidinone (MRX-I) with an improved class safety profile. *J. Med. Chem. 57* (11), 4487−97.

(8) Nagiec, E. E., Wu, L., Swaney, S. M., Chosay, J. G., Ross, D. E., Brieland, J. K., and Leach, K. L. (2005) Oxazolidinones inhibit cellular proliferation via inhibition of mitochondrial protein synthesis. *Antimicrob. Agents Chemother. 49* (9), 3896−902.

(9) McKee, E. E., Ferguson, M., Bentley, A. T., and Marks, T. A. (2006) Inhibition of mammalian mitochondrial protein synthesis by oxazolidinones. *Antimicrob. Agents Chemother. 50* (6), 2042−9.

(10) Roger, C., Roberts, J. A., and Muller, L. (2018) Clinical Pharmacokinetics and Pharmacodynamics of Oxazolidinones. *Clin. Pharmacokinet. 57* (5), 559−575.

(11) De Vriese, A. S., Coster, R. V., Smet, J., Seneca, S., Lovering, A., Van Haute, L. L., Vanopdenbosch, L. J., Martin, J. J., Groote, C. C., Vandecasteele, S., and Boelaert, J. R. (2006) Linezolid-induced inhibition of mitochondrial protein synthesis. *Clin. Infect. Dis. 42* (8), 1111−7.

(12) Lee, E. Y., and Caffrey, A. R. (2018) Thrombocytopenia with Tedizolid and Linezolid. *Antimicrob. Agents Chemother. 62* (1), No. 1453-17, DOI: 10.1128/AAC.01453-17.

(13) Brickner, S. J., Hutchinson, D. K., Barbachyn, M. R., Manninen, P. R., Ulanowicz, D. A., Garmon, S. A., Grega, K. C., Hendges, S. K., Toops, D. S., Ford, C. W., and Zurenko, G. E. (1996) Synthesis and Antibacterial Activity of U-100592 and U-100766, Two Oxazolidinone Antibacterial Agents for the Potential Treatment of Multidrug-Resistant Gram-Positive Bacterial Infections. *J. Med. Chem. 39*, 673−679.

(14) Komine, T., Kojima, A., Asahina, Y., Saito, T., Takano, H., Shibue, T., and Fukuda, Y. (2008) Synthesis and Structure - Activity Relationship Studies of Highly Potent Novel Oxazolidinone Antibacterials. *J. Med. Chem. 51*, 6558−6562.

(15) Das, B., Rudra, S., Yadav, A., Ray, A., Rao, A. V., Srinivas, A. S., Soni, A., Saini, S., Shukla, S., Pandya, M., Bhateja, P., Malhotra, S., Mathur, T., Arora, S. K., Rattan, A., and Mehta, A. (2005) Synthesis and

SAR of novel oxazolidinones: discovery of ranbezolid. *Bioorg. Med. Chem. Lett. 15* (19), 4261−7.
(16) Renslo, A. R., Luehr, G. W., and Gordeev, M. F. (2006) Recent developments in the identification of novel oxazolidinone antibacterial agents. *Bioorg. Med. Chem. 14* (12), 4227−40.
(17) Brickner, S. J. (1996) Oxazolidinone antibacterial agents. *Curr. Pharm. Des. 2*, 175−194.
(18) Chellat, M. F., Raguz, L., and Riedl, R. (2016) Targeting Antibiotic Resistance. *Angew. Chem., Int. Ed. 55* (23), 6600−26.
(19) Zhanel, G. G., Love, R., Adam, H., Golden, A., Zelenitsky, S., Schweizer, F., Gorityala, B., Lagace-Wiens, P. R., Rubinstein, E., Walkty, A., Gin, A. S., Gilmour, M., Hoban, D. J., Lynch, J. P., 3rd, and Karlowsky, J. A. (2015) Tedizolid: a novel oxazolidinone with potent activity against multidrug-resistant gram-positive pathogens. *Drugs 75* (3), 253−70.
(20) Im, W. B., Choi, S. H., Park, J. Y., Choi, S. H., Finn, J., and Yoon, S. H. (2011) Discovery of torezolid as a novel 5-hydroxymethyl-oxazolidinone antibacterial agent. *Eur. J. Med. Chem. 46* (4), 1027−39.
(21) Shili, C., R. L, Yusheng, W. U., Jiacheng, Z., and Roger, H. Process for the synthesis of triazoles using heterocyclization, reductive amination and cross-coupling reactions. 2006.
(22) Ebner, D. C., Culhane, J. C., Winkelman, T. N., Haustein, M. D., Ditty, J. L., and Ippoliti, J. T. (2008) Synthesis of novel oxazolidinone antimicrobial agents. *Bioorg. Med. Chem. 16* (5), 2651−6.
(23) Belousoff, M. J., Eyal, Z., Radjainia, M., Ahmed, T., Bamert, R. S., Matzov, D., Bashan, A., Zimmerman, E., Mishra, S., Cameron, D., Elmlund, H., Peleg, A. Y., Bhushan, S., Lithgow, T., and Yonath, A. (2017) Structural Basis for Linezolid Binding Site Rearrangement in the Staphylococcus aureus Ribosome. *mBio 8* (3), No. 395-17, DOI: 10.1128/mBio.00395-17.
(24) Flanagan, S., McKee, E. E., Das, D., Tulkens, P. M., Hosako, H., Fiedler-Kelly, J., Passarell, J., Radovsky, A., and Prokocimer, P. (2015) Nonclinical and pharmacokinetic assessments to evaluate the potential of tedizolid and linezolid to affect mitochondrial function. *Antimicrob. Agents Chemother. 59* (1), 178−85.
(25) Zheng, J., Chen, Z., Lin, Z., Sun, X., Bai, B., Xu, G., Chen, J., Yu, Z., and Qu, D. (2020) Radezolid Is More Effective Than Linezolid Against Planktonic Cells and Inhibits Enterococcus faecalis Biofilm Formation. *Front. Microbiol. 11*, 196.
(26) Dolomanov, O. V., Bourhis, L. J., Gildea, R. J., Howard, J. A. K., and Puschmann, H. (2009) OLEX2: a complete structure solution, refinement and analysis program. *J. Appl. Crystallogr. 42*, 339−341.
(27) Sheldrick, G. M. (2015) Crystal structure refinement with SHELXL. *Acta Crystallogr., Sect. C: Struct. Chem. 71*, 3−8.
(28) Sheldrick, G. M. (2015) SHELXT - Integrated space-group and crystal-structure determination. *Acta Crystallogr., Sect. A: Found. Adv. 71*, 3−8.
(29) Li, X., Mooney, P., Zheng, S., Booth, C. R., Braunfeld, M. B., Gubbens, S., Agard, D. A., and Cheng, Y. (2013) Electron counting and beam-induced motion correction enable near-atomic-resolution single-particle cryo-EM. *Nat. Methods 10* (6), 584−90.
(30) Zheng, S. Q., Palovcak, E., Armache, J. P., Verba, K. A., Cheng, Y., and Agard, D. A. (2017) MotionCor2: anisotropic correction of beam-induced motion for improved cryo-electron microscopy. *Nat. Methods 14* (4), 331−332.
(31) Zhang, K. (2016) Gctf: Real-time CTF determination and correction. *J. Struct. Biol. 193* (1), 1−12.
(32) Wagner, T., and Raunser, S. (2020) The evolution of SPHIRE-crYOLO particle picking and its application in automated cryo-EM processing workflows. *Commun. Biol. 3* (1), 61.
(33) Wagner, T., Merino, F., Stabrin, M., Moriya, T., Antoni, C., Apelbaum, A., Hagel, P., Sitsel, O., Raisch, T., Prumbaum, D., Quentin, D., Roderer, D., Tacke, S., Siebolds, B., Schubert, E., Shaikh, T. R., Lill, P., Gatsogiannis, C., and Raunser, S. (2019) SPHIRE-crYOLO is a fast and accurate fully automated particle picker for cryo-EM. *Commun. Biol. 2*, 218.
(34) Zivanov, J., Nakane, T., Forsberg, B. O., Kimanius, D., Hagen, W. J., Lindahl, E., and Scheres, S. H. (2018) New tools for automated high-resolution cryo-EM structure determination in RELION-3. *eLife 7*, No. 42166, DOI: 10.7554/eLife.42166.
(35) Punjani, A., Rubinstein, J. L., Fleet, D. J., and Brubaker, M. A. (2017) cryoSPARC: algorithms for rapid unsupervised cryo-EM structure determination. *Nat. Methods 14* (3), 290−296.
(36) Phillips, J. C., Braun, R., Wang, W., Gumbart, J., Tajkhorshid, E., Villa, E., Chipot, C., Skeel, R. D., Kale, L., and Schulten, K. (2005) Scalable molecular dynamics with NAMD. *J. Comput. Chem. 26* (16), 1781−802.
(37) Liebschner, D., Afonine, P. V., Baker, M. L., Bunkoczi, G., Chen, V. B., Croll, T. I., Hintze, B., Hung, L. W., Jain, S., McCoy, A. J., Moriarty, N. W., Oeffner, R. D., Poon, B. K., Prisant, M. G., Read, R. J., Richardson, J. S., Richardson, D. C., Sammito, M. D., Sobolev, O. V., Stockwell, D. H., Terwilliger, T. C., Urzhumtsev, A. G., Videau, L. L., Williams, C. J., and Adams, P. D. (2019) Macromolecular structure determination using X-rays, neutrons and electrons: recent developments in Phenix. *Acta Crystallogr. D Struct Biol. 75* (Pt 10), 861−877.
(38) Emsley, P., Lohkamp, B., Scott, W. G., and Cowtan, K. (2010) Features and development of Coot. *Acta Crystallogr., Sect. D: Biol. Crystallogr. 66* (4), 486−501.
(39) Schrödinger (2010) *The PyMOL Molecular Graphics System*, version 1.3r1, Schrödinger, LLC

https://dx.doi.org/10.1021/acsptsci.0c00041
ACS Pharmacol. Transl. Sci. 2020, 3, 425−432

ChemPubSoc Europe

DOI: 10.1002/cmdc.201900042

CHEMMEDCHEM Communications

Check for updates

cryoEM-Guided Development of Antibiotics for Drug-Resistant Bacteria

Matthew J. Belousoff,[a] Hari Venugopal,[b] Alexander Wright,[c] Samuel Seoner,[c] Isabella Stuart,[a] Chris Stubenrauch,[a] Rebecca S. Bamert,[a] David W. Lupton,*[c] and Trevor Lithgow*[a]

While the ribosome is a common target for antibiotics, challenges with crystallography can impede the development of new bioactives using structure-based drug design approaches. In this study we exploit common structural features present in linezolid-resistant forms of both methicillin-resistant *Staphylococcus aureus* (MRSA) and vancomycin-resistant *Enterococcus* (VRE) to redesign the antibiotic. Enabled by rapid and facile cryoEM structures, this process has identified (*S*)-2,2-dichloro-*N*-((3-(3-fluoro-4-morpholinophenyl)-2-oxooxazolidin-5-yl)methyl)acetamide (LZD-**5**) and (*S*)-2-chloro-*N*-((3-(3-fluoro-4-morpholinophenyl)-2-oxooxazolidin-5-yl)methyl) acetamide (LZD-**6**), which inhibit the ribosomal function and growth of linezolid-resistant MRSA and VRE. The strategy discussed highlights the potential for cryoEM to facilitate the development of novel bioactive materials.

Combating antimicrobial resistance requires multiple therapeutic strategies, including the discovery of new molecular scaffolds, re-engineering and repurposing of existing drugs, in addition to improvements in antimicrobial stewardship.[1] The discovery of small molecules with antimicrobial activity can be facilitated by structure-based drug design (SBDD) strategies.[2] Approaches of this type exploit structural information, obtained using various biochemical assays, to drive the drug design process. Although a number of techniques are employed in SBDD, the field remains heavily reliant on X-ray[3] and NMR-based analysis,[4] techniques with orthogonal advantages with regard to resolution, throughput, and analysis cost. With the emergence of high-resolution cryoEM as a powerful tool for determining structural information, its ability to be applied in SBDD, particularly when examining biomolecules poorly suited to X-ray analysis, has been discussed extensively.[5] In addition to reaching resolution targets that allow unambiguous placement of small molecules, cryoEM is a solution-phase technique which may prove advantageous. Although cryoEM-guided design of novel ligands is underdeveloped, the interactions of known drugs with their targets have been examined with the *Plasmodium* 20S proteasome,[6] the GPCR family,[7] pathogenic ribosomes,[8] receptor-bound insulin,[9] and important HIV viral entry proteins,[10] to name a few examples. In 2017, Scheres, Baum, and co-workers exploited cryoEM to elucidate the mode of action that mefloquine uses to inhibit the *Plasmodium falciparum* ribosome, and then used this insight to develop a next-generation molecule with enhanced antiparasitic activity.[11] As part of our studies into mechanisms of antibiotic resistance, we examined one of the escape routes that *Staphylococcus aureus* uses to develop resistance to the ribosomal-interfering antibiotic, linezolid.[8a] These studies, and those of others,[12] show that disparate mutations result in a common structural rearrangement that lowers the affinity of linezolid binding at the peptidyl transferase center (PTC), suggesting that in order to preserve its enzymatic activity, the ribosome is not infinitely malleable.[8a,12a,13] Taking advantage of these common structural changes in linezolid-resistant (Lin^R) strains, we postulated that simple modification of an amide group in linezolid should reintroduce binding to the altered A-site. Herein we report studies on this topic which have exploited cryoEM to guide the development of new linezolid analogues that target Lin^R strains of MRSA and VRE. Central to this work was a cryoEM workflow that allowed rapid delivery of high-resolution structural information. This strategy should have potential value in many areas of SBDD.

The bacterial ribosome is a common target for drug development, with over 40% of antibiotics in clinical use targeting its activity in protein synthesis.[14] The first-in-class oxazolidinone antibiotic[15] linezolid is one of the most recently introduced drugs. Linezolid is widely used for the treatment of infections caused by bacterial resistance to antibiotics such as methicillin and vancomycin, particularly MRSA and VRE.[13a,16] Linezolid binds to rRNA in the A-site of the peptidyl transferase center of the ribosome (SI Figure S1), and inhibits protein synthesis by sterically blocking recruitment of aminoacyl-tRNA. As a first step in re-engineering a form of linezolid that could bind and inhibit the altered A-site in Lin^R strains, we examined the characteristics of the compacted drug-binding site in the Lin^R ribosome. A large conformational change of the rRNA residues U^{2506} and G^{2505} (*E. coli* numbering used throughout) was observed, which in turn remodels the linezolid-binding pocket

[a] *Dr. M. J. Belousoff, I. Stuart, Dr. C. Stubenrauch, R. S. Bamert, Prof. T. Lithgow*
Infection and Immunity Program, Department of Microbiology, Monash University, Clayton 3800 (Australia)
E-mail: trevor.lithgow@monash.edu

[b] *H. Venugopal*
Ramaciotti Centre for Electron Microscopy, Monash University, Clayton 3800 (Australia)

[c] *A. Wright, S. Seoner, Prof. D. W. Lupton*
School of Chemistry, Monash University, Clayton 3800 (Australia)
E-mail: david.lupton@monash.edu

Supporting information and the ORCID identification number(s) for the author(s) of this article can be found under: https://doi.org/10.1002/cmdc.201900042.

© 2019 Wiley-VCH Verlag GmbH & Co. KGaA, Weinheim

(Figure 1 a, SI Figure S2 a). Comparative analysis of these various mutant ribosomes revealed a highly similar conformation in most of the rRNA residues, raising the prospect that an induced-fit mode of binding may be possible in the peptidyl transferase pocket. The largest conformational change in the Lin^R ribosome structure impacted the position of the oxazolidinone heterocycle (SI Figure S1 a). In a linezolid:70S ribosome complex, the amide carbonyl group points toward G^{2447}, making a putative hydrogen bond with A^{2451} (SI Figure S2 b). A rational analysis of the structural coordinates for the Lin^R ribosome (SI Figure S2) revealed binding opportunities for an amide at the 5-position if it were redirected toward A^{2503}, where a larger pocket is present that could potentially accommodate a bulkier amide than the acyl group present in linezolid (SI Figure S2). If such reorientation could be achieved, then linezolid-based analogues should prove capable of evading contraction-based drug resistance. To address this hypothesis, a selection of amides at the 5-position of linezolid starting with the common amine (*S*)-5-(aminomethyl)-3-(3-fluoro-4-morpholinophenyl)oxazolidone-2 (**2**) itself,[17] were prepared (Figure 1 b).

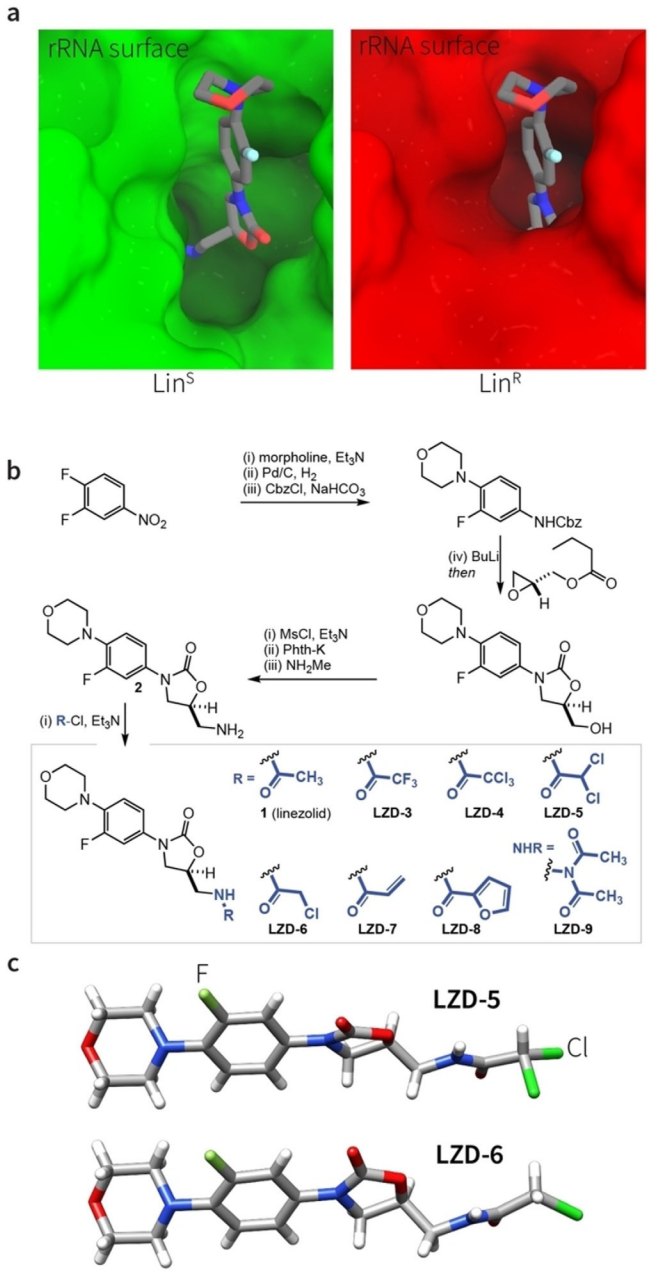

Figure 1. a) View of the drug-binding pocket from the cryoEM structures of the 70S ribosomes from Lin^S (PDB ID: 5TCU and EMDB EMD-8402; left panel) and Lin^R (PDB ID: 5T7V and EMDB EMD-8369; right panel) MRSA strains. Overlaid is the binding position of linezolid. Green and red surfaces are the solvent-accessible surface of the rRNA about the site of linezolid binding. b) Synthetic scheme used to synthesise LZD-**3**–**9**.[17] c) Stick representation of the X-ray crystal structures of LZD-**5** and LZD-**6**.

While the compounds displayed in Figure 1 would not necessarily be viable clinical antibiotics due to undesirable pharmacokinetics (solubility) and pharmacodynamics (potential toxicity; LZD-**7** being a potential Michael acceptor and the halogenated compounds containing labile leaving groups), they were selected to examine the viability of cryoEM as a tool of value for targeting ligand biomolecule interactions.

Screening the compounds in a minimal inhibitory concentration (MIC) assay demonstrated that the compounds were active as antibiotics in vitro (Table 1). The chloro (LZD-**6**) and dichloro (LZD-**5**) derivatives were the most active in inhibiting growth of Lin^R MRSA. These compounds bind to both the linezolid-sensitive (Lin^S) and Lin^R states of the drug-binding pocket on the ribosome, as they inhibit both Lin^S and Lin^R strains of *S. aureus* (Table 1). X-ray crystallographic analysis of LZD-**5** and LZD-**6** (Figure 1 c, SI Figure S3) showed a similar overall structure, with both crystallising in the same space group with very similar unit cells (SI Table S1). Both showed a "linear" topology with two molecules exhibiting a head-to-tail van der Waals interaction, which formed the basis of the asymmetric unit of the crystal lattice. The 2-oxazolidone moiety of both LZD-**5** and LZD-**6**, lying in the same plane as the fluorinated aromatic ring (although LZD-**5** showed a greater offset between the plane of the aromatic ring and the 2-oxazolidone ring which was 30° compared to 8° in LZD-**6**). None of the other derivatives showed improved activity, while some were significantly worse. For example, the imide derivative LZD-**9** showed relatively poor MIC values for all bacterial strains (Table 1).

Table 1. Minimum inhibitory concentration for antibiotics against relevant bacterial species: *Staphylococcus aureus*, *Staphylococcus capitis*, *Staphylococcus epidermidis*, and vancomycin-resistant *Enterococcus* (VRE, ATCC700221).

Compound	MIC [μg mL^{-1}][a]				
	S. aur.	MRSA (Lin^R)	*S. cap.*	*S. epi.*	VRE
linezolid	0.5	2	0.5	0.25	1
LZD-**3**	1	4	1	1	2
LZD-**4**	2	4	1	1	2
LZD-**5**	0.5	1	0.25	0.25	0.5
LZD-**6**	0.25	1	0.25	0.13	0.25
LZD-**7**	1	2	1	0.5	1
LZD-**8**	2	8	2	2	4
LZD-**9**	4	16	2	2	4

[a] MIC assays were carried out according to CLSI protocols.[18]

© 2019 Wiley-VCH Verlag GmbH & Co. KGaA, Weinheim

To assess whether the improved potency of LZD-**5** and LZD-**6** was driven by more effective inhibition of ribosomal activity, we assayed the compounds in a cell-free translation system. In this system, synthesis of firefly luciferase is used to monitor ribosomal activity using a luminescence readout. LZD-**5** and LZD-**6** were more effective at inhibiting protein synthesis by the ribosome than was the parent compound linezolid (Table 2).

Table 2. Ribosome activity determined in a luciferase transcription/translation assay.

Compound	IC_{50} [μM][a]
linezolid	3.8 ± 0.3
LZD-**3**	6 ± 1
LZD-**4**	3.9 ± 0.7
LZD-**5**	2.6 ± 0.2
LZD-**6**	2.6 ± 0.5
LZD-**7**	5 ± 1
LZD-**8**	> 40
LZD-**9**	> 30

[a] IC_{50} plots are provided in Supporting Information Figure S8; values are the mean ± SEM ($n = 3$).

To determine if the improved activity was due to the foreshadowed conformational changes, single-particle cryoEM data was collected yielding refined maps for LZD-**5**:70S and LZD-**6**:70S to a global resolution of 3.1 and 2.8 Å, respectively (SI Figure S4a). As the molecules of interest bind in the 50S ribosomal subunit, Euler angle refinement was focused on the 50S subunit. This allowed well-resolved maps around the peptidyl transferase center, with the local resolutions around the area of interest both being < 2.9 Å (SI Figure S4 b, c). Given reports that use of the Volta Phase Plate (VPP) may lead to more facile visualisation of small bound ligands due to its higher contrast micrographs (SI Figure S5 a),[20] the LZD-**5**:70S structure was collected using a VPP, while the LZD-**6**:70S was collected using a standard varied defocus strategy. Both maps are strikingly similar, with the atomic structures superimposable (SI Figure S3). Using the VPP collection we were able to collect high-quality data (SI Figure S5 b, c), which resulted in similar resolution (SI Figure S2 a, b) but with significantly fewer micrographs (SI Table S2). By periodic movement of the VPP, we were able to keep the phase shift within suitable boundaries (SI Figure S5 d, e) leading to high-quality reconstructions (SI Figure S5 f) and similar map quality (SI Figure S6 a) to the varied defocus collection. This means a substantial decrease in valuable microscope time to achieve equally high-quality and interpretable data for unambiguous drug placement in the ribosome.

The density map around LZD-**6** was interpretable at 2.8 Å resolution, and the position and stereochemistry of the molecule could be placed unambiguously (Figure 2 a). LZD-**6** adopts a similar binding position to that of linezolid (Figure 2 b); however, the 2-chloroacyl group is now directed toward rRNA residue A^{2503} and the 2-oxazolidone ring is in a slightly different orientation to maximise hydrophobic interactions with U^{2504} and accommodate the different acyl group position (Figure 2 c). Relative to the crystal structure of LZD-**6** alone, which adopts a linear topology, the acyl tail rotates around the amide bond to form more favorable interactions with the surrounding rRNA when in complex with the ribosome. This different mode of binding shows that there is a degree of flexibility in the binding of the oxazolidinone pharmacophore to the PTC, and that the representative linezolid binding[19] is not the only rigid option for this family of antibiotics.

In the ribosome, LZD-**6** is assisted by additional interactions with surrounding rRNA residues (Figure 2 d). The 2-chloroacyl group forms a hydrogen bond with the ribose of A^{2503}, while a hydrophobic interaction with the purine of A^{2503}, and a π–π interaction with the purine of G^{2061} are also gained (Figure 2 e). These interactions allow the 2-oxazolidone ring to form a favorable hydrophobic interaction with pyrimidine of U^{2504}. All other interactions with the morpholine and the fluorophenyl ring are similar to linezolid, except that the morpholine ring in LZD-**5** and LZD-**6** forms a hydrogen bond with the ribose of A^{2451}. These observations also provide a potential explanation for why tedizolid, a new oxazolidinone antibiotic, effectively binds the ribosome without having a morpholine, as it might promote an induced fit at a similar location to interact with A^{2451} via a hydrogen bond between tedizolid's pyridine ring and the ribose sugar.[21]

While LZD-**6** had two-fold greater ability to inhibit bacterial growth, we set out to examine if the decreased MIC activity correlated with any decrease in the acquisition of drug resistance. The evolution of resistance toward LZD-**6** by *S. aureus* was determined by serially passaging *S. aureus* through broth containing various concentrations of LZD-**6**. After 16 days of serial passaging on 0.5 μg mL^{-1} LZD-**6**, a spontaneous mutant was isolated. This mutant was cultured and shown to be drug-resistant *S. aureus* by serial broth microdilution, yielding a MIC value of 2 μg mL^{-1}. The rate at which the drug-resistant *S. aureus* evolved is ≈1 cell per $< 10^8$ generations, which is more rapid than the observed rate of ≈1 cell per $< 10^{10}$ generations for the parent compound, linezolid. However, it was found that while the MIC value of the resistance mutant was four-fold greater than the starting strain, the LZD-**6** resistance phenotype came with a mild fitness cost, as evidenced by a slower growth phenotype (SI Figure S7 a, b). This fitness versus resistance cost had an even more profound effect when we generated resistance mutants by long-period static growth at sub-MIC concentrations of LZD-**6** (SI Figure S7 c, d).

Medicinal chemistry approaches to developing antibiotics, particularly targeting the ribosome, can be hampered by challenges gaining structural information from which to design novel compounds. Exploiting knowledge of structural changes in the ribosomal drug-binding pocket that gives rise to linezolid resistance in MRSA, we have designed analogues of linezolid that overcome these changes, thereby binding and inhibiting the Lin^R ribosome. There is reason to believe that in vivo, the evolution of resistance to LZD-**5** and LZD-**6** will be more challenging to bacteria, given that these compounds bind through an induced fit into both states (i.e., Lin^S and Lin^R) of the drug-binding pocket and given that the active site of the ribosome

© 2019 Wiley-VCH Verlag GmbH & Co. KGaA, Weinheim

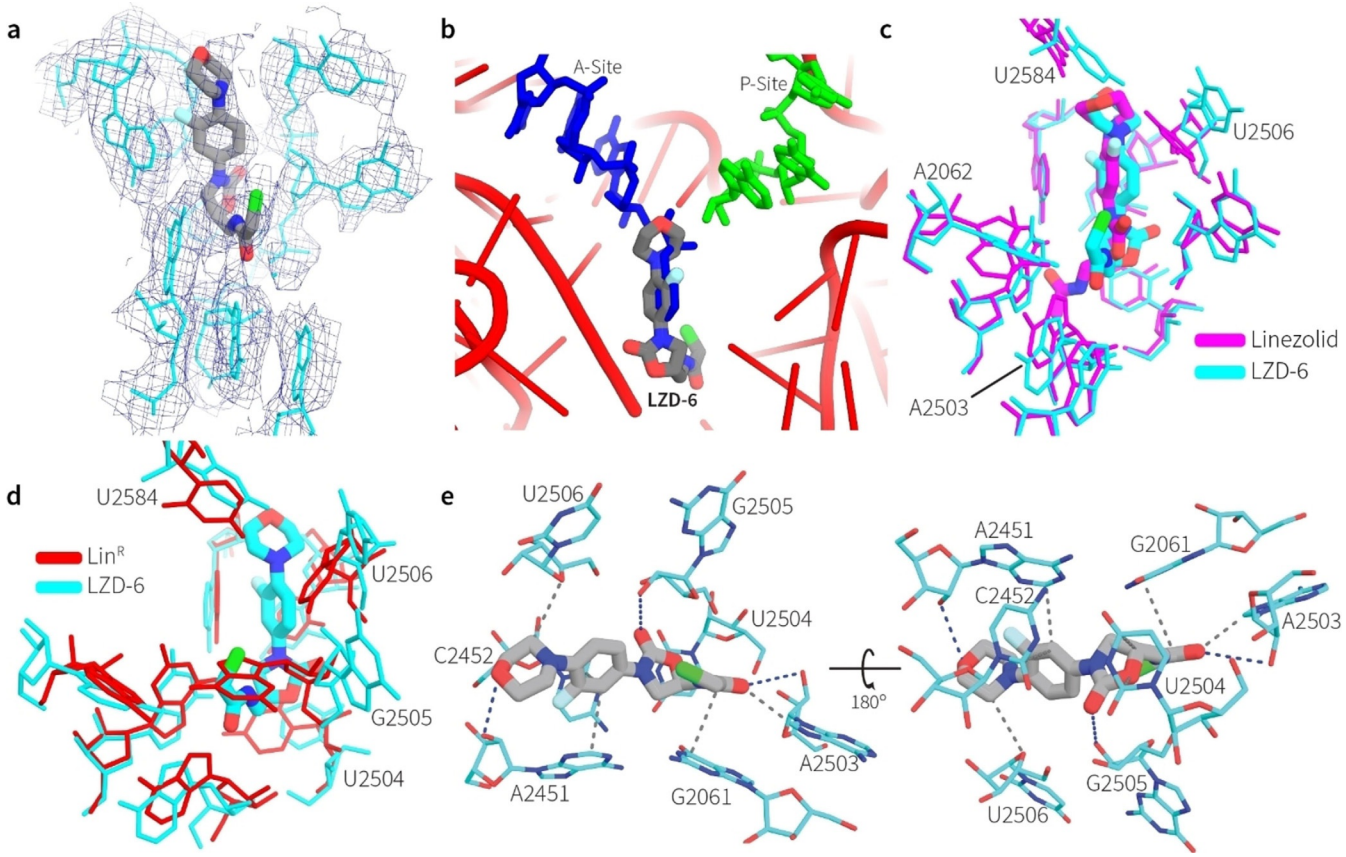

Figure 2. a) Diagrammatic representation of the cryoEM structure of the peptidyl transferase center in the 50S ribosomal subunit from MRSA with LZD-**6** bound at the peptidyl transferase center,[19] highlighting how LZD-**6** would inhibit protein synthesis by blocking binding of incoming tRNA into the A-site. Overlaid are the positions of the 3′ end of the tRNAs in the A-site and P-site (blue and green, respectively). b) CryoEM density map drawn at 4σ around the binding site of LZD-**6** in the A-site of the peptidyl transferase center (PTC). Stick representations show the rRNA residues; thicker sticks show the oxazolidine molecule. c) Cartoon representation of the structural superposition of the binding region of the LZD-**6**:70S complex (cyan) and the linezolid:70S complex (magenta) structure (PDB ID: 4WFA).[19] d) Cartoon representation of the structural superposition of the binding region of both the LZD-**6**:70S complex (cyan) and the same region of the Lin^R ribosome structure (red) from MRSA (PDB ID: 5T7V)[8a] e) Enlargement of the binding site of LZD-**6** (grey and CPK coloring) in the drug-binding pocket, showing in dotted lines interactions with surrounding rRNA residues (blue: hydrogen bond interactions; grey: van der Waals/π–π interactions); left and right are 180° rotations about the viewing plane.

where the compounds bind is not infinitely malleable and that there is an observable growth fitness cost that coincides with resistance. Structural analysis of the modified drug bound to the ribosome showed how these modified structures induced a fit to the ribosome through additional interactions with rRNA residues in the binding pocket. This work showcases the use of cryoEM as a framework for the rational design of new antibiotics. Although LZD-**5** and **6** are unlikely to display drug-like features, ongoing work in our laboratories is focused on the use of cryoEM to provide facile access to structural information of value to the pursuit of novel antibiotics.

Experimental Section

Detailed method descriptions are available in the Supporting Information. All figures were generated with either PyMOL or UCSF Chimera. The atomic structures have been deposited in the RCSB Protein Data Bank with accession codes 6DDD for LZD-**5**–MRSA50S and 6DDG for LZD-**6**–MRSA50S. The cryoEM density maps were deposited in the Electron Microscopy Data Bank under accession codes EMD-7867 for LZD-**5**–MRSA50S and EMD-7870 for LZD-**6**–MRSA50S.

Acknowledgements

We acknowledge the support staff and facilities at the Monash Ramaciotti Centre for Cryo-Electron Microscopy. We thank Georg Ramm for Titan Krios support, Anton Peleg for providing clinical isolates of MRSA and VRE, and Ana Traven and Jamie Rossjohn for comments on the manuscript. We acknowledge the NVIDIA Corporation for donating GPUs to aid with calculations used in this research. This work was supported by the Multi-modal Australian ScienceS Imaging and Visualisation Environment (MASSIVE) (www.massive.org.au). The work was funded by the National Health & Medical Research Council of Australia (Program Grant 1092262 to T.L.) and the Australia Research Council (DP 170103567 to D.W.L.). The funders had no role in study design, data collection and interpretation, or the decision to submit the work for publication.

© 2019 Wiley-VCH Verlag GmbH & Co. KGaA, Weinheim

Conflict of interest

The authors declare no conflict of interest.

Keywords: antibiotic resistance · cryoEM · linezolid · structure-based drug design

[1] a) D. Brown, *Nat. Rev. Drug Discovery* **2015**, *14*, 821 – 832; b) A. Du Toit, *Nat. Rev. Microbiol.* **2016**, *14*, 725; c) V. W. Soo, B. W. Kwan, H. Quezada, I. Castillo-Juarez, B. Perez-Eretza, S. J. Garcia-Contreras, M. Martinez-Vazquez, T. K. Wood, R. Garcia-Contreras, *Curr. Top. Med. Chem.* **2017**, *17*, 1157 – 1176.

[2] K. J. Simmons, I. Chopra, C. W. Fishwick, *Nat. Rev. Microbiol.* **2010**, *8*, 501 – 510.

[3] a) T. L. Blundell, H. Jhoti, C. Abell, *Nat. Rev. Drug Discovery* **2002**, *1*, 45 – 54; b) A. C. Anderson, *Chem. Biol.* **2003**, *10*, 787 – 797.

[4] a) D. A. Erlanson, S. W. Fesik, R. E. Hubbard, W. Jahnke, H. Jhoti, *Nat. Rev. Drug Discovery* **2016**, *15*, 605 – 619; b) D. C. Rees, M. Congreve, C. W. Murray, R. Carr, *Nat. Rev. Drug Discovery* **2004**, *3*, 660 – 672.

[5] a) G. Scapin, C. S. Potter, B. Carragher, *Cell Chem. Biol.* **2018**, *25*, 1318 – 1325; b) A. Merk, A. Bartesaghi, S. Banerjee, V. Falconieri, P. Rao, M. I. Davis, R. Pragani, M. B. Boxer, L. A. Earl, J. L. S. Milne, S. Subramaniam, *Cell* **2016**, *165*, 1698 – 1707; c) X. C. Bai, G. McMullan, S. H. Scheres, *Trends Biochem. Sci.* **2015**, *40*, 49 – 57; d) F. Merino, S. Raunser, *Angew. Chem. Int. Ed.* **2017**, *56*, 2846 – 2860; *Angew. Chem.* **2017**, *129*, 2890 – 2905.

[6] H. Li, M. Bogyo, P. C. da Fonseca, *FEBS J.* **2016**, *283*, 4238 – 4243.

[7] Y. L. Liang, M. Khoshouei, M. Radjainia, Y. Zhang, A. Glukhova, J. Tarrasch, D. M. Thal, S. G. B. Furness, G. Christopoulos, T. Coudrat, R. Danev, W. Baumeister, L. J. Miller, A. Christopoulos, B. K. Kobilka, D. Wootten, G. Skiniotis, P. M. Sexton, *Nature* **2017**, *546*, 118 – 123.

[8] a) M. J. Belousoff, Z. Eyal, M. Radjainia, T. Ahmed, R. S. Bamert, D. Matzov, A. Bashan, E. Zimmerman, S. Mishra, D. Cameron, H. Elmlund, A. Y. Peleg, S. Bhushan, T. Lithgow, A. Yonath, *MBio* **2017**, *8*, e00395-17; b) N. Fischer, P. Neumann, A. L. Konevega, L. V. Bock, R. Ficner, M. V. Rodnina, H. Stark, *Nature* **2015**, *520*, 567 – 570.

[9] G. Scapin, V. P. Dandey, Z. Zhang, W. Prosise, A. Hruza, T. Kelly, T. Mayhood, C. Strickland, C. S. Potter, B. Carragher, *Nature* **2018**, *556*, 122 – 125.

[10] D. Lyumkis, J. P. Julien, N. de Val, A. Cupo, C. S. Potter, P. J. Klasse, D. R. Burton, R. W. Sanders, J. P. Moore, B. Carragher, I. A. Wilson, A. B. Ward, *Science* **2013**, *342*, 1484 – 1490.

[11] W. Wong, X. C. Bai, B. E. Sleebs, T. Triglia, A. Brown, J. K. Thompson, K. E. Jackson, E. Hanssen, D. S. Marapana, I. S. Fernandez, S. A. Ralph, A. F. Cowman, S. H. W. Scheres, J. Baum, *Nat. Microbiol.* **2017**, *2*, 17031.

[12] a) K. S. Long, B. Vester, *Antimicrob. Agents Chemother.* **2012**, *56*, 603 – 612; b) J. B. Locke, M. Hilgers, K. J. Shaw, *Antimicrob. Agents Chemother.* **2009**, *53*, 5265 – 5274.

[13] a) R. Bi, T. Qin, W. Fan, P. Ma, B. Gu, *J. Global Antimicrob. Resist.* **2017**, *13*, 11 – 19; b) T. A. Cidral, M. C. Carvalho, A. M. Figueiredo, M. C. de Melo, *APMIS* **2015**, *123*, 867 – 871; c) S. Tsiodras, H. S. Gold, G. Sakoulas, G. M. Eliopoulos, C. Wennersten, L. Venkataraman, R. C. Moellering, M. J. Ferraro, *Lancet* **2001**, *358*, 207 – 208.

[14] a) J. Poehlsgaard, S. Douthwaite, *Nat. Rev. Microbiol.* **2005**, *3*, 870 – 881; b) D. N. Wilson, *Nat. Rev. Microbiol.* **2014**, *12*, 35 – 48; c) J. Lin, D. Zhou, T. A. Steitz, Y. S. Polikanov, M. G. Gagnon, *Annu. Rev. Biochem.* **2018**, *87*, 451 – 478.

[15] K. J. Shaw, M. R. Barbachyn, *Ann. N. Y. Acad. Sci.* **2011**, *1241*, 48 – 70.

[16] A. M. Bal, M. Z. David, J. Garau, T. Gottlieb, T. Mazzei, F. Scaglione, P. Tattevin, I. M. Gould, *J. Global Antimicrob. Resist.* **2017**, *10*, 295 – 303.

[17] S. J. Brickner, D. K. Hutchinson, M. R. Barbachyn, P. R. Manninen, D. A. Ulanowicz, S. A. Garmon, K. C. Grega, S. K. Hendges, D. S. Toops, C. W. Ford, G. E. Zurenko, *J. Med. Chem.* **1996**, *39*, 673 – 679.

[18] *Clinical and Laboratory Standards Institute (2015) Performance Standards for Antimicrobial Susceptibility Testing, 25th Informational Supplement*, CLSI Document M100-S25, Clinical and Laboratory Standards Institute, Wayne, PA (USA).

[19] Z. Eyal, D. Matzov, M. Krupkin, I. Wekselman, S. Paukner, E. Zimmerman, H. Rozenberg, A. Bashan, A. Yonath, *Proc. Natl. Acad. Sci. USA* **2015**, *112*, E5805 – E5814.

[20] O. von Loeffelholz, G. Papai, R. Danev, A. G. Myasnikov, S. K. Natchiar, I. Hazemann, J. F. Menetret, B. P. Klaholz, *J. Struct. Biol.* **2018**, *202*, 191 – 199.

[21] G. G. Zhanel, R. Love, H. Adam, A. Golden, S. Zelenitsky, F. Schweizer, B. Gorityala, P. R. Lagace-Wiens, E. Rubinstein, A. Walkty, A. S. Gin, M. Gilmour, D. J. Hoban, J. P. Lynch III, J. A. Karlowsky, *Drugs* **2015**, *75*, 253 – 270.

Manuscript received: January 20, 2019
Accepted manuscript online: January 22, 2019
Version of record online: February 12, 2019

© 2019 Wiley-VCH Verlag GmbH & Co. KGaA, Weinheim

A structurally characterized *Staphylococcus aureus* evolutionary escape route from treatment with the antibiotic linezolid.

Laura Perlaza-Jiménez[1,2+], Kher-shing Tan[1,2+], Sarah Piper[3], Rachel Johnson[3], Rebecca Bamert[1,2], Alexander Wright[5], David Lupton[5], Trevor Lithgow[1,2*] & Matthew J. Belousoff[2,3,4*]

1. Centre to Impact AMR, Monash University, Wellington Rd, Clayton 3800, Australia
2. Infection and Immunity Program, Biomedicine Discovery Institute and Department of Microbiology, Monash University, Wellington Rd, Clayton 3800, Australia
3. Drug Development Biology, Monash Institute of Pharmaceutical Sciences, Parkville, 3052, Australia
4. Centre for Cryo-electron Microscopy of Membrane Proteins, Monash Institute of Pharmaceutical Sciences, Monash University, Parkville 3052, Australia
5. School of Chemistry, Monash University, Wellington Rd, Clayton 3800, Australia

+ Authors contributed equally to the manuscript
* Corresponding authors: trevor.lithgow@monash.edu, matthew.belousoff@monash.edu

Keywords: antimicrobial resistance, MRSA, antibiotics, ribosomes, cryoEM

ABSTRACT

Methicillin resistant *Staphylococcus aureus* (MRSA) is a bacterial pathogen that presents genuine health concern. Treatment requires use of last line antibiotics such as members of the oxazolidone family, of which linezolid is the first member of this class to see regular use in the clinic. This work reports a small-scale linezolid resistance selection experiment whereby strains of MRSA were subjected to antibiotic selection. Clonal isolates that exhibited linezolid resistance were isolated and their genomes were sequenced. Resistant mutants were isolated which accumulated mutations in the ribosomal protein uL3. A particular clone which had two mutations in uL3 exhibited resistance to linezolid, two-fold higher than the clinical breakpoint. Ribosomes from this strain were isolated and subjected to single particle cryo electron microscopic analysis and compared to the parent strain. It was found that the mutations in uL3 lead to a rearrangement of a loop that makes contact with Helix90, propagating a structural change over 15 Å away to the binding site of the antibiotic, which swings U2504 into the binding site of the antibiotic, leading to antibiotic resistance.

INTRODUCTION

Bacterial infection is a massive burden on modern healthcare with significant human and financial cost (REF). Treatment of bacterial infections with antibiotics is increasingly compromised due to the evolution of antimicrobial resistant (AMR) phenotypes in bacteria such as *Staphylococcus aureus*, which appears in many nosocomial infections as well as wound related infections (REF). The Centers for Disease Control rates the evolution of AMR phenotypes in *S. aureus* as an urgent threat to human health, and the rapid evolution of methicillin-resistant *S. aureus* (MRSA) coupled with high rates of community acquired MRSA promoted the need to use more potent antibiotics. Linezolid was the first fully synthetic antibiotic, introduced into clinical use in 2000 (REF). Due to observations of sporadic outbreaks of linezolid-resistance, further compounds of the oxazolidone class of antibiotics such as tedizolid, radezolid and contezolid are now being developed. However, the use of these second-generation oxazolidones too is promoting MRSA clones to adapt and evolve resistance (REF), requiring a reevaluation of how readily and for what reasons *S. aureus* can accommodate to breakthrough the bacteriostatic effect of oxazolidone antibiotics. Given that linezolid- and tedizolid-resistance in MRSA are considered to be uncommon relative to other antimicrobial resistance (AMR) phenotypes in MRSA (REF), the time for re-evaluation of this resistance is now.

Linezolid acts by inhibiting ribosome function at the peptidyl transferase center (PTC) by sterically blocking the 'A-site' for incoming 3′ amino acylated tRNA docking into the 50S subunit of the bacterial ribosome (REF). Thus, the presence of linezolid directly impacts on the core process of protein synthesis. Studies with MRSA *in vitro* have revealed that short exposure to linezolid induces a stress response, resulting in an initial adaptation to the drug. This adaptive response is characterized by the transcriptional profile of 18 sRNAs when MRSA is grown for 30 minutes in the presence of sub-MIC concentrations of linezolid (REF). While none of these small RNAs impact on the growth rates of MRSA in rich brain-heart infusion (BHI) medium, nor change the linezolid sensitivity as judged by MIC assays, the expectation is that these sRNAs mediate a network of proteomic changes to protect MRSA during growth in the presence of the antibiotic. Whole genome sequencing (WGS) studies investigating longer term exposure to linezolid, in the context of human treatments, revealed mutations causative of linezolid-resistance are found only in genes encoding the 23S rRNA (REF). Recent studies carried out in human patients suggest that, in the course of linezolid treatment of an MRSA infection, as little as 14 days is required to see a linezolid-

resistant clone evolve and take over the population of MRSA at the infection site (REF). Across 32 isolates subject to WGS analysis in one study in Taiwan, linezolid-resistance was attributed to a G2576T (*Escherichia coli* numbering of rRNA nucleotides used throughout) variant in the 23S rRNA (REF) and a G2576T variant independently evolved in a human infection study in France (REF) and another in Japan (REF). This nucleotide is located in the PTC and impacts directly on the shape of the linezolid-binding site (REF).

While resistance to linezolid may be considered a rare event (REF), even a slow increase in linezolid-resistance is of concern given its status as a last-line antibiotic. In this study, we used *in vitro* selection over an extended (x days) timeline to select for linezolid resistance in MRSA. WGS analysis determined mutations corresponded to linezolid resistance were found in clones that had severe fitness defects readily detected through growth phenotype assays. Single-particle cryoEM analysis of the 50S ribosomal subunit showed that the linezolid resistant mutations in the gene encoding ribosomal protein L3 delivered the same structural defect as previously reported for mutations in the 23S rRNA suggesting that, in structural terms, a common escape mechanism defines linezolid-resistant MRSA and that this comes at a fitness cost that can be exploited therapeutically.

RESULTS AND DISCUSSION

To assess the prominent mutational landscape around linezolid resistance we performed a selection experiment on ATCC43300, a type strain of MRSA which is sensitive to oxazolidone antibiotics. This strain is in clinical use as a reference standard for antimicrobial susceptibility testing and quality control evaluation of Mueller-Hinton Agar (REF). The selection experiment was performed using a standard Brain Heart Infusion (BHI) broth, where a static culture was inoculated with 10^8 colony forming units (cfu) of MRSA and treated with sub-MIC concentration of linezolid (Figure 1A). Once growth was observed in the static culture, selection was applied by streaking out onto BHI-agar plates containing concentrations of linezolid above or below the MIC. If colonies grew on the selection plates, they were re-cultured, stored and at least 3 of these colonies were used for a further round of selection.

Clones from the selection experiments were tested for growth phenotype in three relevant bacterial media: BHI broth, Luria-Bertani (LB) broth and Mueller Hinton broth. After one generation of selection on linezolid there was a significant delay in growth on BHI media for the first generation strain xX, and a small but significant defect in growth rate. For the third generation strain xX, both the delayed lag phase and the diminished growth rate were even more profound in all three growth media (Figure 1B). These data are consistent with and quantify previous observations of that linezolid-resistant MRSA strains have a small colony phenotype when plated on solid media (REF), demonstrating that linezolid-resistance comes at a fitness cost in MRSA.

Seventeen of the evolved clones were subject to WGS using Illumina short-read sequencing. As expected with the long term nature of the selection experiment, a number of single nucleotide variations (SNVs) were identified in each genome (Supplementary Table S1). To be certain that these had arisen in the course of this experiment, the ancestral strain ATCC43300 was sequenced in parallel and used for comparison. There are no physical hot-spots for mutation, with the SNVs are distributed around the genome (Figure 2A). The SNVs accumulate over the course of the generations, with the first generation strains A1, B1 and C1 each having ... SNVs and the second and third generation strains having progressively more mutation. However, we note that in order to establish themselves for growth on linezolid, the

three first generation strains have 45 SNVs in common, and these changes were inherited and maintained in all subsequent generations (Figure 2B). These SNVs are located in …….

Only in one case did we identify two SNVs in a single open-reading frame, with these occurring in the gene encoding ribosomal protein L3 (Figure 2C). The 70S ribosome in *S. aureus* is composed of 46 ribosomal proteins and the 16S rRNA and 23S rRNA (REF). Analysis of the open-reading frame sequences for all of the ribosomal proteins and the rRNA sequences identified only a single mutation in the first generation strain xX, corresponding to G155R change in ribosomal protein L3 (Figure 2C). Further rounds of selection had generated a strain of MRSA, strain xX, with a phenotype that exceeded the clinical break-point definition of linezolid-resistant (MIC of 8 µg/µL; Table 1). Strain xX was characterized by the G155R mutation in combination with M169I mutation.

To further understand the effects of these mutations on the oxazolidinone binding site and the overall topology of the PTC we isolated ribosomes from both the ancestral ATCC43300 strain and strain xX. Both samples of ribosomes were subject to single-particle cryoEM, imaged in a cryoTEM equipped with a direct electron camera. In the context of 70S ribosome particles, a final masked refinement of the 50S subunits using the RELION software package (REF) yielded maps resolved to 3.0 and 3.1 Å for the ATCC43300 and strain xX structures respectively (see Supp Figure S1 and Table 2). This map resolution is high enough for unambiguous assignments for both the mutation site and nearby PTC (Figure 3).

The impact of the G155R, M169I double mutation on the loop of ribosomal protein L3 that contacts rRNA helix 90 is striking (Figure 3B, 3C, 3D). Most notable is the drastic change in the overall fold in the loop around the G155R position (Figure 3C, 3D). The impact of this change in ribosomal protein L3 forces helix 90 of the 23S rRNA to form such that C2512 is moved out of its helical arrangement (Figure 3D). The second mutation M169I is on the other side of the loop in ribosomal protein L3. The overall effect of the M169I mutation is primarily the further rearrangement around C2512, propagating the structural change further along helix 90 and culminating in an adjustment of the position of U2504 (Figure 3E). U2504 is both a key residue in the oxazolidinone binding site and also plays a vital role in protein synthesis, forming part of the A-site wall in the PTC (REF). This structural change leaves no space for linezolid binding on the ribosome.

Mutations in the gene encoding ribosomal protein L3 are prevalent in linezolid-resistant MRSA, and two previous studies have addressed distinct L3 mutations in terms of structural impact (REFs). A ……. that did what to ribosomal protein L3 (REF), and a deletion of residue S145 from ribosomal protein L3 caused it to …….. (REF). In each case, the same structural propagation effect was established on the surrounding rRNA.

Linezolid-resistant phenotypes have been reported to be enhanced by acquisition of new genes such as *cfr* which encodes a methylase that modifies A2503 in the 23S rRNA or genes that permit hypermutation in the *rrl* locus (REF). Other direct SNPs in all 5 copies of the *rrl* (23S rRNA encoding) regions can be established and maintained to provide a linezolid-resistant phenotype (REF). We suggest that an important determinate in initial, early stages of antibiotic escape remains those select SNV mutations in ribosomal protein L3 that can transmit physical changes through the rRNA to rearrange the linezolid binding site. Structural analysis suggests that all of these provide linezolid resistance through a common rearrangement binding site of linezolid and other oxazolidones (REF), and we suggest that this structural rearrangement comes with a concomitant cost to bacterial fitness. New combination therapies or other strategies to exploit this weakness in linezolid-resistant MRSA should be pursued.

MATERIALS AND METHODS

In vitro selection experiment

A type MRSA strain (*Staphylococcus aureus* subsp. *aureus* Rosenbach, ATCC 43300) was used as the ancestral strain for the *in vitro* selection. The experiment was modelled on a protocol described by Peleg and co-workers[1]. Briefly a starting culture in BHI broth was streaked onto BHI-agar plates, where a single colony was picked and grown BHI broth (5 mL) for 24 hours with shaking. 20 mL of BHI (containing 0, 2, 4 and 8 µg/mL linezolid) were then inoculated with 10^8 colony forming units (c.f.u), grown under static conditions at 37 °C and monitored over several days until the broth became cloudy suggesting bacterial growth. To select bacteria that had acquired a stable linezolid-resistant phenotype, the culture was diluted in BHI (1:10, 1:100, 1:1000) and plated for colony growth on BHI-agar supplemented with either 0, 2, 4 or 8 µg/mL linezolid. Colonies were counted using a Phenobooth (Singer Instruments), and the cells stored frozen at -80 °C for whole genome sequencing.

Bacterial growth and MIC assays

Growth analysis by monitoring absorbance at 600 nm as a function of time is described by Belousoff *et al.*[2]. MIC assays on the mutants generated in the *in vitro* selection experiments were carried out as previously described [3]. Kher-shing to add any further details?

While genome sequencing and sequence analysis

Kher-shing/Laura to fill out?

Purification of 70S ribosomes

70S ribosomes were isolated from the type MRSA strain (ATCC43300) and from Strain xX that displayed resistance to linezolid at 8 µg/mL. The methods for ribosome isolation were previously described be Belousoff *et al.*[4].

Vitrified sample preparation and data collection

Samples of the 70S ribosomes were concentrated to 0.3 mg/mL. Aliquots of 3 µL were applied to a glow-discharged Quantifoild R1.2/1.3 200 mesh holey grid (Quantifoil GmbH, Großlöbichau, Germany) and were flash frozen in liquid ethane using the Vitrobot mark IV (Thermo Fisher Scientific) set at 100% humidity and 4 °C for the prep chamber with a blot time of 1.5 s. Data were collected on a Glacios TEM (Thermo Fisher Scientific) operated at an

accelerating voltage of 200 kV with a 50 μm C2 aperture with no objective aperture inserted and at an indicated magnification of 120 kx in nanoprobe TEM mode. A Falcon 3 direct electron detector positioned post column was used to acquire dose fractionated images of the samples, the exposure time was 40 seconds yielding an electron dose of 47.5 e.Å^{-2}. Movies were recorded in gain normalized mode with the experimental parameters listed in **Table S1** using a 9-hole position beam-image shift acquisition pattern in using the EPU software package (Thermo Fisher Scientific).

Data processing

Micrographs were motion corrected using UCSF MotionCor2[5] and dose weighted averages had their CTF parameters estimated using gCTF[6]. Particles were picked in using the Laplacian of Gaussian picker in the RELION (version 3.1) software package[7-9]. These particles were extracted from the micrographs and subjected to 2D classification and ab initio 3D and 3D refinement in RELION. The resulting homogeneous particle selections then underwent 3D refinement, particle polishing and CTF envelop fitting in RELION. A mask was then prepared which covered the most of the 50S subunit, and a focussed final 3D refinement was performed to yield the final maps of the 50S subunit for each of the two structures.

Modelling into cryoEM maps

The coordinates of the 50S subunit from the PDB:5TCU[4] were used as the starting point for the models described in this work. Manual adjustment of the residues that were different from the deposited structure were performed in the coot software package[10] and rigid body fitted into the cryoEM maps using the SITUS software package[11]. The models were then flexibly fitted into the density using Molecular Dynamics Flexible Fitting (MDFF) as implemented in namd2[12] and the resulting structures were then further refined in real space using Phenix[13,14] along with manual curation in coot. See **Table 2** for the molecular modelling statistics.

Model analysis

Interactions and structure comparisons were carried out using PyMOL Molecular Graphics System, Version 2.3 (Schrödinger, LLC) and figures were generated in either PyMOL or UCSF Chimera[15].

REFERENCES

1 Peleg, A. Y. *et al.* Whole genome characterization of the mechanisms of daptomycin resistance in clinical and laboratory derived isolates of Staphylococcus aureus. *PLoS One* **7**, e28316, doi:10.1371/journal.pone.0028316 (2012).

2 Belousoff, M. J. *et al.* cryoEM-Guided Development of Antibiotics for Drug-Resistant Bacteria. *ChemMedChem* **14**, 527-531, doi:10.1002/cmdc.201900042 (2019).

3 Belousoff, M. J. *et al.* Crystal structure of the synergistic antibiotic pair, lankamycin and lankacidin, in complex with the large ribosomal subunit. *Proc Natl Acad Sci U S A* **108**, 2717-2722, doi:10.1073/pnas.1019406108 (2011).

4 Belousoff, M. J. *et al.* Structural Basis for Linezolid Binding Site Rearrangement in the Staphylococcus aureus Ribosome. *MBio* **8**, doi:10.1128/mBio.00395-17 (2017).

5 Zheng, S. Q. *et al.* MotionCor2: anisotropic correction of beam-induced motion for improved cryo-electron microscopy. *Nat Methods* **14**, 331-332, doi:10.1038/nmeth.4193 (2017).

6 Zhang, K. Gctf: Real-time CTF determination and correction. *Journal of structural biology* **193**, 1-12, doi:10.1016/j.jsb.2015.11.003 (2016).

7 Zivanov, J. *et al.* New tools for automated high-resolution cryo-EM structure determination in RELION-3. *Elife* **7**, doi:10.7554/eLife.42166 (2018).

8 Fernandez-Leiro, R. & Scheres, S. H. W. A pipeline approach to single-particle processing in RELION. *Acta Crystallogr D Struct Biol* **73**, 496-502, doi:10.1107/S2059798316019276 (2017).

9 Scheres, S. H. RELION: implementation of a Bayesian approach to cryo-EM structure determination. *Journal of structural biology* **180**, 519-530, doi:10.1016/j.jsb.2012.09.006 (2012).

10 Emsley, P., Lohkamp, B., Scott, W. G. & Cowtan, K. Features and development of Coot. *Acta Crystallogr D Biol Crystallogr* **66**, 486-501, doi:10.1107/S0907444910007493 (2010).

11 Wriggers, W. Conventions and workflows for using Situs. *Acta Crystallogr D* **68**, 344-351, doi:10.1107/S0907444911049791 (2012).

12 Phillips, J. C. *et al.* Scalable molecular dynamics with NAMD. *Journal of computational chemistry* **26**, 1781-1802, doi:10.1002/jcc.20289 (2005).

13 Afonine, P. V. *et al.* Real-space refinement in PHENIX for cryo-EM and crystallography. *Acta Crystallogr D Struct Biol* **74**, 531-544, doi:10.1107/S2059798318006551 (2018).

14 Adams, P. D. *et al.* PHENIX: a comprehensive Python-based system for macromolecular structure solution. *Acta Crystallogr D Biol Crystallogr* **66**, 213-221, doi:10.1107/S0907444909052925 (2010).

15 Pettersen, E. F. *et al.* UCSF Chimera--a visualization system for exploratory research and analysis. *Journal of computational chemistry* **25**, 1605-1612, doi:10.1002/jcc.20084 (2004).

ACKNOWLEDGEMENTS
This work was supported by grants from US-DOD (PRMRP: W81XWH1910126) for M.J.B. and by the National Health & Medical Research Council of Australia (Program Grant 1092262 to T.L.) and the Australia Research Council (DP 170103567 to D.W.L.). The funders had no role in study design, data collection, and interpretation, or the decision to submit the work for publication. We acknowledge the support from Thermo Scientific for the Glacios housed in at the Bio21 Institute, Melbourne University as part of a collaboration with Prof. Patrick Sexton and Assoc. Prof. Denisse Wootten's laboratory. This work was supported by the MASSIVE HPC facility (www.massive.org.au).

AUTHOR CONTRIBUTIONS
L.P and K-S. T. carried out adaptation experiments and analyzed genomic data. S.P., R.J., R.B. analyzed cryoEM data and helped with structural modelling. A.W and D.L. provided linezolid for selection experiments, T.L and M.J.B. came up with experimental design, performed data analysis and interpretation and T.L, M.J.B, R.B and L.P. prepared the manuscript. M.J.B. prepared ribosome samples and collected the cryoEM data.

FIGURE LEGENDS

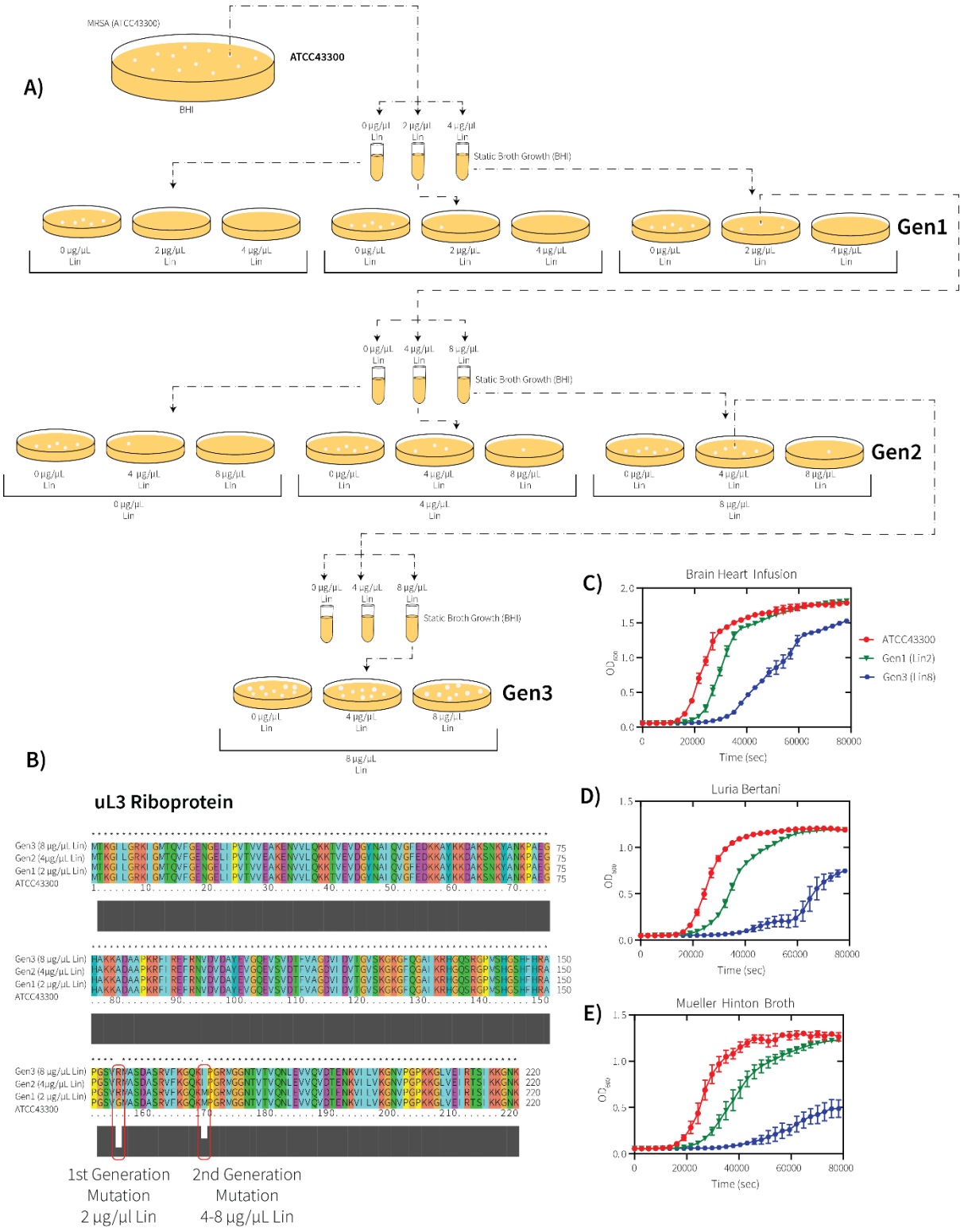

Figure 1. Selection for linezolid antibiotic resistance in *S. aureus*.

A) Overall schematic of linezolid resistance selection experiment. Briefly a single colony of *S. aureus* (ATCC43300) is grown under static growth conditions at 37 °C until growth is observed. These are then plated out on Brain Heart Infusion Agar plates at increasing linezolid concentration. If colonies form on the agar plates, the colony is then passaged through another round of static growth at various concentrations of linezolid and the process

is repeated until there is confluent growth on the 8 μg/μL linezolid BHI-agar. Clones had their gDNA sequenced at each generation. **B)** Growth curves of the ancestral ATCC43300 (red trace), Strain xX (green trace) and Strain xX (blue trace) in Brain Heart Infusion broth (top panel), in Luria Bertani broth (middle panel) and in Mueller Hinton broth (bottom panel).

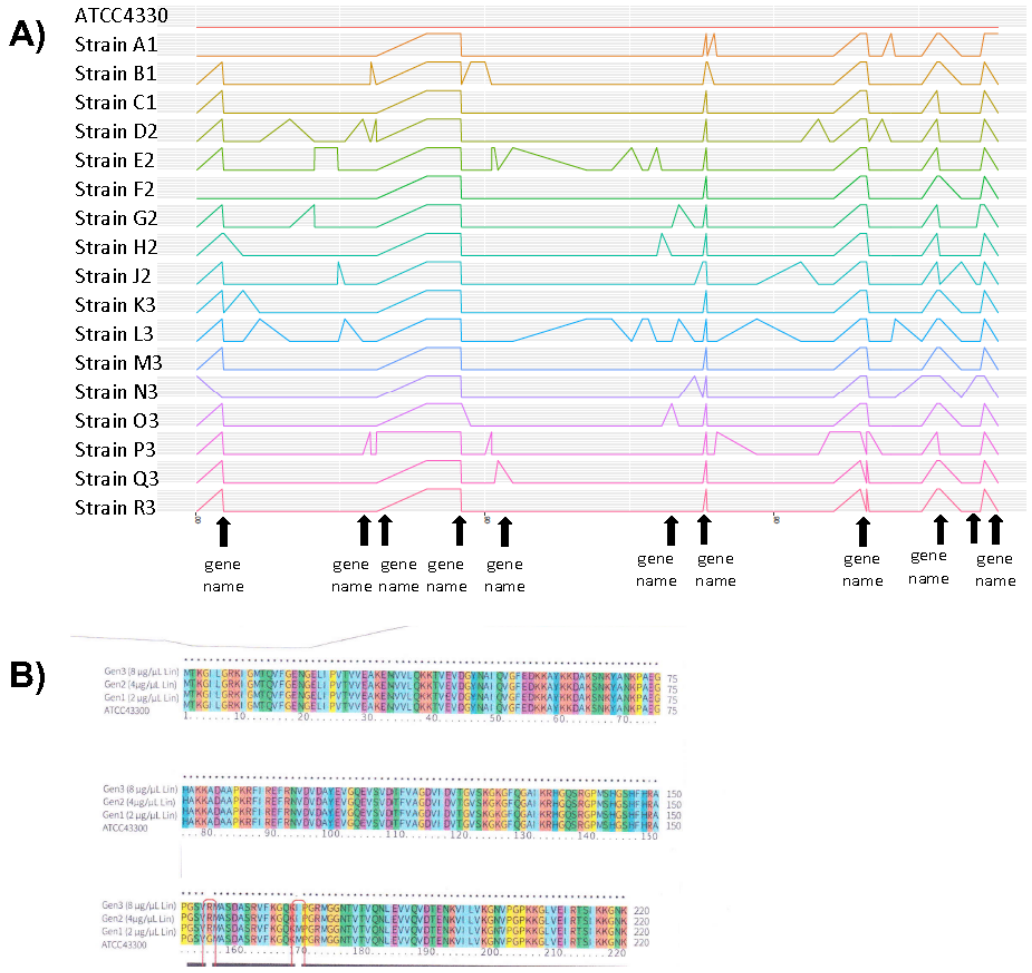

Figure 2. Mutations that give rise to linezolid resistant phenotypes.
A) Genome comparisons for the ancestral ATCC43300 strain and the seventeen evolved strains analyzed by WGS. The peaks in the coloured lines denote the position of each SNV with respect to the ancestral sequence. Flat-line indicates sequence identity. **B)** Multiple sequence alignment of ribosomal protein L3 in selected clones that exhibited resistance to linezolid at either 2, 4 or 8 µg/µL linezolid at different generations of the selection experiment. Two mutations were observed the first giving rise to moderate linezolid resistance being G155R the second mutation M169I yielding the clinical linezolid resistance breakpoint.

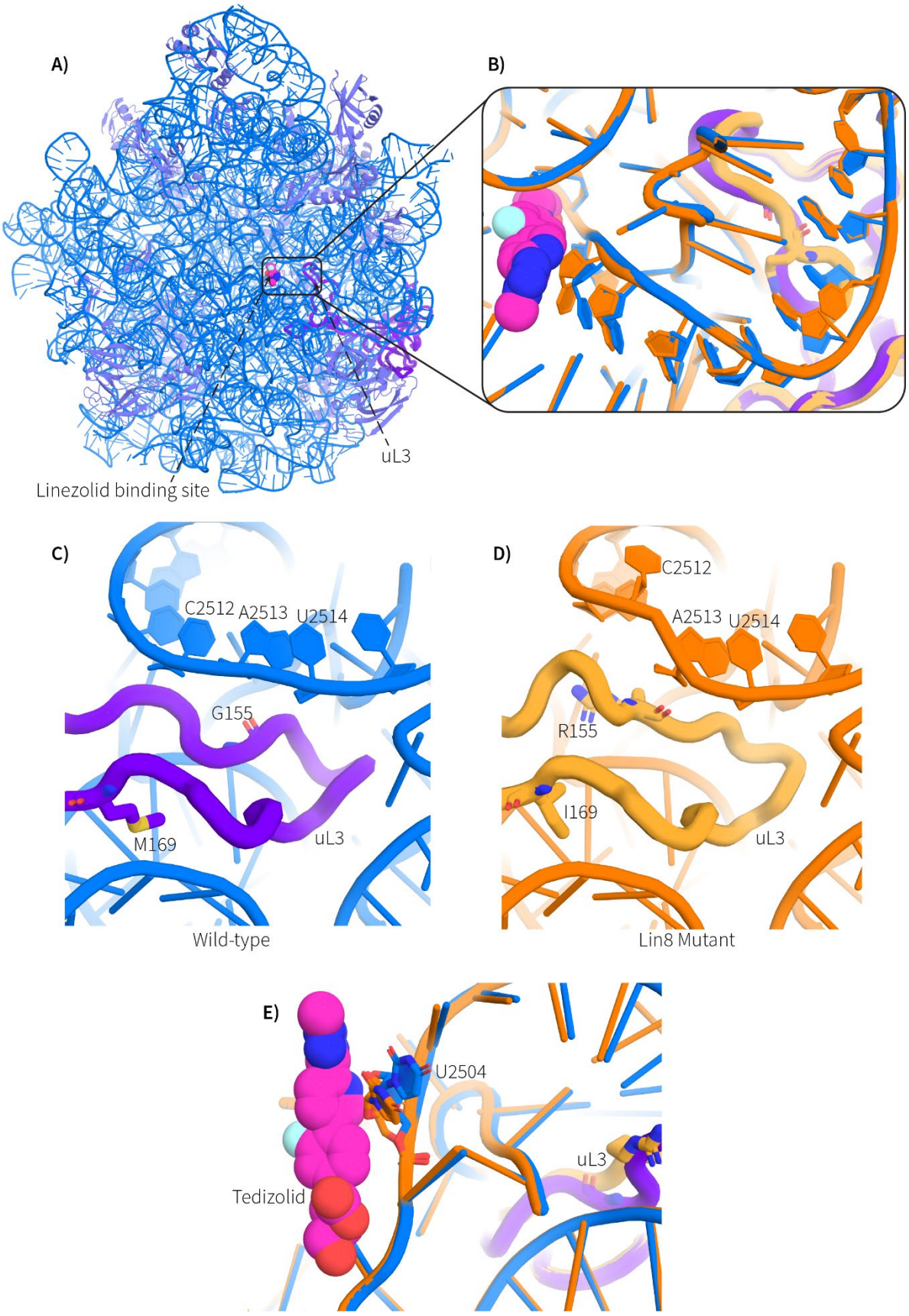

Figure 3. CryoEM structural analysis of the 50S ribosome of *S. aureus*.
A) Crown view of the 50S ribosome from *S. aureus* ATCC43300. Overlaid is the binding position of linezolid (REF). Shown in blue is the rRNA, in magenta are the ribosomal

proteins, and in deep purple is ribosomal protein L3. **B)** Magnification of the linezolid binding site, with linezolid drawn as pink spheres. Overlaid are both the ATCC4330 (blue, with L3 shown in purple) and strain xX structure (orange/straw for L3). Note the structural propagation along Helix 90 all the way to the peptidyl transferase centre (PTC) and linezolid binding site. **C)** ATCC43300 ribosome structure centred on the ribosomal protein L3 (purple) loop that makes contact with Helix90 (blue). Note that the G155 makes close contact with A2513 (*E. coli* numbering). **D)** Strain xX ribosome structure from the same view of the uL3 loop as in panel (C). Drawn in straw is the uL3 protein loop and the mutation sites are depicted in stick representation. Note the G155R mutation changes the overall topology of the N-terminal side of the uL3 loop which changes its interaction with Helix90, introducing a rearrangement of C2512. **E)** Overlay of the ATCC43300 ribosome (blue/purple) and strain xX ribosome (orange/straw) structures centred on the oxazolidone binding site. Drawn in pink spheres is the oxazolidone drug tedizolid (REF). Shown is nucleobase U2504 which has moved out to where the oxazolidone core binds, reducing the steric volume available for oxazolidone binding.

Table 1. MIC assessments for the evolved MRSA strains.

Strain	**MIC** (ug/mL)	**Clinical designation**	**L3 mutation**
ATCC43300	xxx	Sensitive	None
Strain A1	xxx	Sensitive	None
Strain B1	xxx	Sensitive	None
Strain C1	xxx		None
Etc.			

Table 2. Data collection and refinement statistics.

Data Collection	**ATCC43300**	**Strain xX**
Micrographs	2583	2749
Electron dose (e^-/A^2)	47.5	47.5
Voltage (kV)	200	200
Exposure time (sec)	40	40
Detector	Falcon3	Falcon3
Pixel size (Å)	0.895	0.895
Defocus range (μm)	0.5-1.5	0.5-1.5
Symmetry imposed	C1	C1
Particles (final map)	157k	307.6k
Resolution (0.143 FSC)(Å)	3.0	3.1
Refinement		
CC_{map_model}	0.80	0.78
Map sharpening B factor ($Å^2$)	-54	-41
Model Quality		
R.M.S. deviations		
Bond length (Å)	0.002	0.002
Bond angles (°)	0.447	0.525
Ramachandran		
Favoured (%)	96.43	95.70
Outliers (%)	0	0
Rotamer outliers	0	0.04
C-Beta deviations (%)	0	0
Clashscore	6.24	3.89

SUPPLEMENT

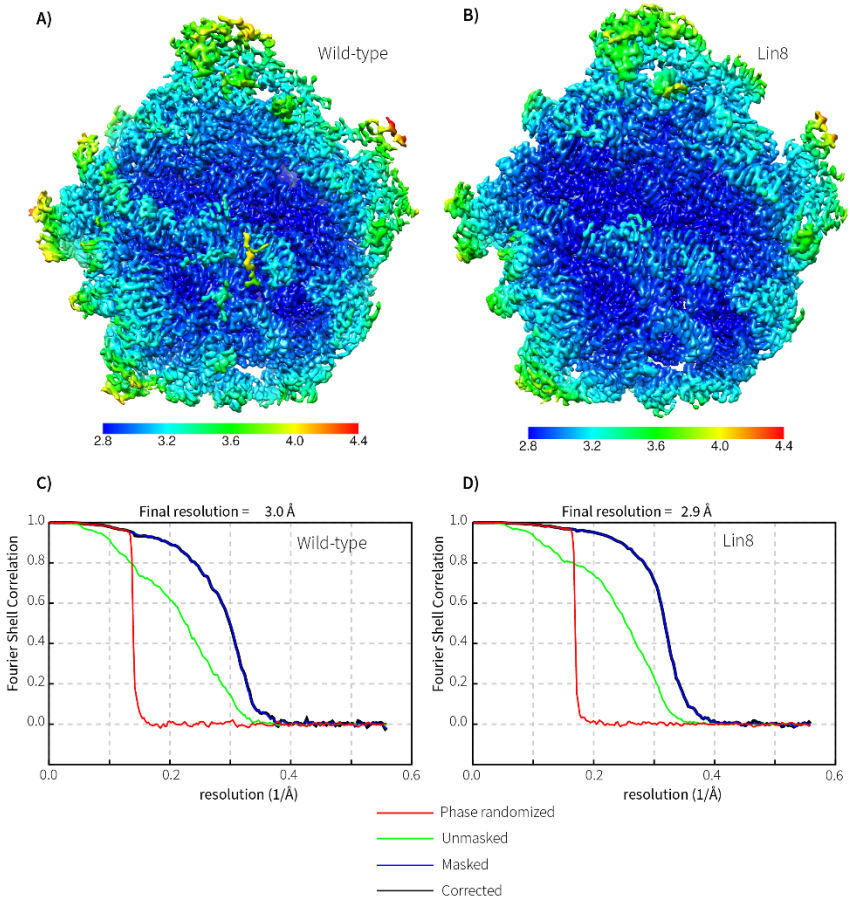

Supplemental Figure S1. CryoEM validation and map quality. **A)** Local Resolution map of the 50S ribosomal subunit for the WT ATCC43300 *S. aureus*. **B)** Local Resolution map of the 50S ribosomal subunit for the Lin8 *S. aureus* strain. **C)** Fourier Shell Correlation (FSC) plots for the WT 50S focussed map. **D)** FSC plots for the Lin8 50S focussed map.